Matching of corroded defects in onshore pipelines based on In-Line Inspections and Voronoi partitions

Rafael Amaya-Gómez, Franck Schoefs, Mauricio Sánchez-Silva, Felipe Muñoz, Emilio Bastidas-Arteaga

Please cite this paper as: Amaya-Gómez R, Schoefs F, Sánchez-Silva M, Muñoz F, Bastidas-Arteaga E. (2022). Matching of corroded defects in onshore pipelines based on In-Line Inspections and Voronoi partitions. Reliability Engineering & System Safety, 223(2022) 108520, https://doi.org/10.1016/j.ress.2022.108520

Matching of corroded defects in onshore pipelines based on In-Line Inspections and Voronoi partitions

Rafael Amaya-Gómez[a,b,*], Franck Schoefs[b], Mauricio Sánchez-Silva[c], Felipe Muñoz[d], Emilio Bastidas-Arteaga[e]

[a] *Chemical Engineering Department, Universidad de los Andes, Cra 1E No. 19A-40, Bogotá, Colombia*
[b] *Université de Nantes, GeM, Institute for Research in Civil and Mechanical Engineering CNRS UMR 6183, Nantes, France*
[c] *Department of Civil & Environmental Engineering, Universidad de los Andes, Cra 1E No. 19A-40, Bogotá, Colombia*
[d] *Empresa Colombiana de Petróleos (ECOPETROL), Cra 7 No. 32-42, Bogotá, Colombia*
[e] *Laboratory of Engineering Sciences for Environment, UMR CNRS 7356, La Rochelle University, France*

Abstract

Onshore pipelines are usually subjected to a corrosion attack. Regular inspections known as In-Line inspections (ILI) are commonly used with magnetic (MFL) or ultrasonic (UT) tools to prevent any failure. New defects will appear between consecutive inspections due to the aggressiveness of the surroundings and the detection thresholds associated with the defects' depth. This work focuses on the matching problem between two inspections, aiming to identify the degradation increments and the position of new defects. Typically, it is linked to the well-known point matching problem in pattern recognition, where the objective is finding the best affine transformation between two sets of points in a plane. This work presents an alternative using Voronoi cells to filter possible matches and an iterative approach to determine the best affine transformation, considering the uncertainty in any direction. The approach was implemented for a real pipeline 45 km long and for synthetic corrosion defects, allowing us to identify possible matches easily. Based on the *new* and *old* defects, some insights about the probability of detection and false alarm are deduced. For this purpose, experimental probability and results from recognized exponential and log-logistic functions were considered.

Keywords: Corroded pipeline, New defects, matching, Probability of detection, Voronoi cells

1. Introduction

Onshore pipelines are critical components in the chain of production and distribution of oil and gas. These pipelines are generally subjected to extreme operation and environmental conditions that would lead to significant corrosion failure risks [1–4]. Therefore, condition assessment though inspections is crucial to ensure adequate levels of serviceability and safety. Corroded pipelines are commonly inspected with Magnetic (MFL) or ultrasonic (UT) tools following In-Line Inspection (ILI). These inspections provide the location and the extent of the metal loss detected based on the pipeline abscissa (longitudinal direction) and a 12-hour clock analogy for the circumferential position. This information is used to monitor the evolution of the corrosion attack every 2 to 6 years to support future maintenance and repair decisions. The challenge lies in the fact that these measurements are subjected to different uncertainties associated with the existence, position, and magnitude of the corrosion defects; for instance, ILI tools have a detection threshold of the depth of the defects near 10% of the wall thickness. Although ILI tools include this threshold, the detection problem does not follow a binary output where every defect above it would be indeed detected. On the contrary, there is a detection error in terms of the probability of being detected (PoD) and being a false alarm (PFA) [5]. These probabilities are intrinsically correlated with the reported accuracy for the defect depth measurements, where it follows that the depth of the defects reported by ILI (d_{ILI}) is related to the real depth (d_{real}) by $d_{ILI} = d_{real} \pm 0.1t$ at 80% certainty.

*Corresponding author,
Email address: r.amaya29@uniandes.edu.co (Rafael Amaya-Gómez)

Other uncertainties include shifted positions and the appearance of new defects possibly caused by a noise signal, complicating any direct matching between consecutive inspections to monitor the pipeline's condition. These new defects can be associated, on the one hand, with the aggressiveness of the surrounding soil, fluid operation, and fluid properties [6]. Several authors agreed that corrosion is favored when the resistivity is reduced regarding soil aggressiveness. Besides, it can be affected by the soil porosity, and groundwater conductivity [7]. Whereas the flow velocity, Zhang and co-workers have obtained that a low flow velocity (< 2 m/s) may lead to a competition between the corrosive species and the inhibitor, and at high velocities (> 6 m/s), an erosion-corrosion may be favored [8]. On the other hand, the new corrosion defects can appear due to a miss-detection in the first inspection or a false alarm in the second one. The reason why new defects appear is unknown without field measurements, but there is certainly an "indication" of a new corrosion point based on the reported in the ILI measurement.

Matching these corrosion defects is associated with the well-known point-matching problem for pattern recognition. This problem seeks an affine transformation using translation, scaling, and rotation parameters to match the highest number of pairs between the two inspection results. There are some available alternatives in this regard for pattern recognition, such as the Iterative Closest Point (ICP) of Besl & McKay [9] or the Thin Plate Spline Robust Matching (TPS-RPM) of Chui & Rangarajan [10]. For corroded pipelines, Dann & Dann [11] proposed a modified version of the TPS-RPM approach, considering possible displacements of the corrosion between inspections based on an Annealing algorithm. This approach seeks an affine transformation matrix with defined rotation, translation, and scaling factors. Considering the uncertainty in the results of the inspection, regarding the longitudinal and circumferential location of corrosion defects, it might be possible that the final matching may not be completely described by this transformation. This work presents an alternative framework to identify which points are classified as *new* and *old* defects using Voronoi partitions to filter preliminary matches and an iterative matching transformation. This framework is applied to a real pipeline of 45 km and synthetic corrosion defects. The approach incorporates location uncertainties and correspondence analysis with outlier filtering. The results in the real and synthetic measurements highlight this framework to be considered by pipeline operators in further condition-based monitoring. The result also allows us to discuss some insights into how this probability can be estimated using the depths of the *new* defects.

The document is structured as follows: Section 2 describes the point-matching problem and the main matching alternatives for pattern recognition. Section 3 introduces the matching alternative for the corroded pipeline and some drawbacks. Section 4 presents the proposed matching approach using a Voronoi partition. Section 5 characterizes the spatial dependencies of the real case study. Section 6 discusses the matching results for the real and synthetic measurements. Section 7 presents some insights about the probability of detection and false alarm, and Section 8 gives the final conclusions.

2. Point matching problem: Identifying new defects between inspections

2.1. General problem formulation

The point matching problem considers two sets of points $\mathcal{P} = \{p_i \in \mathcal{W}, i = 1, 2, \ldots, n\}$ and $\mathcal{Q} = \{q_k \in \mathcal{W}, k = 1, 2, \ldots, m\}$, which represent the defects from the first and second ILI measurement, respectively. In this case, p_i and q_k are vectors containing the location of the pipe and $\mathcal{W} = (\mathbb{A} \times \mathbb{P}) \subset \mathbb{R}^2$ is the plane produced by the abscissa and clock-position once the pipeline is unrolled axially. The traditional point pattern problem search for an affine transformation T for $p_i := (x_{p_i}, y_{p_i})$ given by:

$$T\begin{pmatrix} x_{p_i} \\ y_{p_i} \end{pmatrix} = \begin{pmatrix} t_x \\ t_y \end{pmatrix} + S \begin{pmatrix} \cos\theta & -\sin\theta \\ \sin\theta & \cos\theta \end{pmatrix} \begin{pmatrix} x_{p_i} \\ y_{p_i} \end{pmatrix}, \tag{1}$$

where S is a scaling factor, θ is a rotating angle and t_x and t_y are translations in both main directions. Figure 1 illustrates this matching problem. According to Van Wamelen et al. [12], a matching between the two sets of observations would take place, given a matching probability $\delta \in [0, 1]$ and a matching size $\gamma \in \mathbb{R}$, if there exists a subset of δn points $\mathcal{P}_M$ of $\mathcal{P}$ such that for each $p \in \mathcal{P}_M$ it follows that $\|T(p) - q\| < \gamma$ for a $q \in \mathcal{Q}$.

2.2. Matching alternatives

Point pattern matching is a problem that has been studied before in the field of pattern recognition through different approaches, including fuzzy relaxation, asymmetric neural networks, 2D clustering, and nearest neighbor search

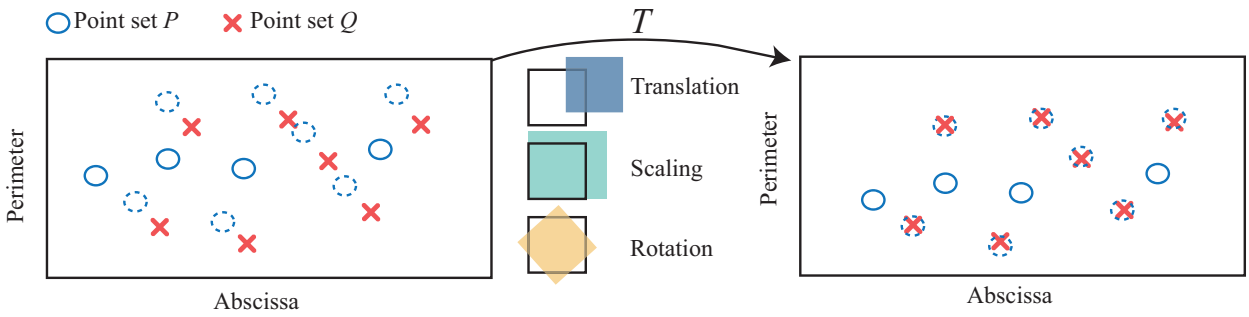

Figure 1: Scheme of the point matching problem.

approaches [12]. Most of these approaches implement a filter approach to determine the number of $\ell \leq \min(n, m)$ of possible matches. One alternative is the Iterative Closest Point (ICP) algorithm that uses the set of nearest neighbors of the points in $\mathcal{P}$ from the points $\mathcal{Q}$, here denoted as $O := \{o_1, \ldots, o_n\}$, in a quaternion-based algorithm that implements an optimal translation $\bar{q}_T$ and rotation $\bar{q}_R = [q_o, q_1, q_2, q_3]^t$ transformations [9]. The latter is associated with a unit quaternion (i.e., $q_o^2 + q_1^2 + q_2^2 + q_3^2 = 1$). The objective is to minimize the following function:

$$f(\bar{q}) = \frac{1}{n}\sum_{i=1}^{n} \|o_i - R(\bar{q}_R)p_i - \bar{q}_T\|^2$$

where $\bar{q} = [\bar{q}_R\, \bar{q}_T]$ and R is the rotation matrix that is produced by the unit quaternion rotation as follows:

$$R = \begin{bmatrix} q_0^2 + q_1^2 - q_2^2 - q_3^2 & 2(q_1q_2 - q_0q_3) & 2(q_1q_3 + q_0q_2) \\ 2(q_1q_2 + q_0q_3) & q_0^2 + q_2^2 - q_1^2 - q_3^2 & 2(q_2q_3 - q_0q_1) \\ 2(q_1q_3 - q_0q_2) & 2(q_2q_3 + q_0q_1) & q_0^2 + q_3^2 - q_1^2 - q_2^2 \end{bmatrix}.$$

Following the closed-solution reported by Horn [13], the optimal rotation transformation $\bar{q}_R$ is determined from the eigenvector of the maximum eigenvalue of the symmetrical matrix whose elements are combinations of sums of products of the point coordinates. Optimal translation $\bar{q}_T$ corresponds with the difference of the centroid of points in $\mathcal{Q}$ (center of mass) and the rotated centroid of points in $\mathcal{P}$. This process follows iteratively until the difference between iterations of the mean square error of the point matching converges to a predefined threshold [9], which can be linked to the accuracy of the location.

Other alternatives consider not only the nearest neighbor, but also the k nearest neighbors of each point in both sets. For instance, the approach reported by Van Wamelen et al. [12] compares the k nearest neighbors of each point p_i with the points in q_k and determines its local affine transformation with the approach reported by Chang et al. [14]. Chang and co-workers proved that if there are ℓ pairs ($\ell \geq 2$) of possible matching points $a_i = (x_{a_i}, y_{a_i}) \leftrightarrow b_i = (x_{b_i}, y_{b_i})$ for $i = 1, \ldots, \ell$, then the affine transformation T that gives the best least-square match that minimizes $\sum_i^{\ell} \|T(a_i) - b_i\|^2$, which is denoted by $\bar{r} = (t_x, t_y, S\cos\theta, S\sin\theta)^t$, is given by [14]:

$$\bar{r} = \frac{1}{det}\begin{bmatrix} l_A & 0 & -\mu_{X_A} & \mu_{Y_A} \\ 0 & l_A & -\mu_{Y_A} & -\mu_{X_A} \\ -\mu_{X_A} & -\mu_{Y_A} & \ell & 0 \\ \mu_{Y_A} & -\mu_{X_A} & 0 & \ell \end{bmatrix}\begin{bmatrix} \mu_{x_B} \\ \mu_{Y_B} \\ l_{A+B} \\ l_{A-B} \end{bmatrix}, \tag{2}$$

where

$$\mu_{X_A} = \sum_i^{\ell} x_{a_i}, \quad \mu_{X_B} = \sum_i^{\ell} x_{b_i}, \quad \mu_{Y_A} = \sum_i^{\ell} y_{a_i}, \quad \mu_{Y_B} = \sum_i^{\ell} y_{b_i}, \tag{3}$$

$$l_{A+B} = \sum_i^{\ell}(x_{a_i}x_{b_i} + y_{a_i}y_{b_i}), \quad l_{A-B} = \sum_i^{\ell}(x_{a_i}y_{b_i} + y_{a_i}x_{b_i}), \quad l_A = \sum_i^{\ell}(x_{a_i}^2 + y_{a_i}^2), \tag{4}$$

$$det = \ell \cdot l_A - \mu_{X_A}^2 - \mu_{Y_A}^2. \tag{5}$$

This transformation is used by Van Wamelen et al. [12] considering as possible matches those points with $\|T(a_i) - b_k\| < \gamma = R_Q/n$ for some a_i and b_k neighbors of p_i and q_k, with R_Q being the minimum disk radius that covers the points in Q. This process continues until a higher number of matches is achieved.

Finally, some approaches implement correspondence matrices with the possibility of outliers from both sets. For instance, the Thin Plate Spline Robust Matching (TPS-RPM) reported by Chui & Rangarajan [10], and the revised version of Yang [15] using a double-sided approach to manage the outliers under a reduced optimization approach, which use an annealing temperature process to solve the optimization problem. Consider a correspondence matrix $\mathbb{C} = [c_{ik}]$ with dimensions $n \times m$ that indicates the probability of matching each $p_i \in \mathcal{P}$ with each $q_k \in Q$. This approach includes two possible outliers vectors r and s with dimensions $(n \times 1)$ and $(1 \times m)$, respectively, associated with the defects that could not be matched in the optimization problem shown in Eq. 6. In this objective function, α and λ are controlling parameters to avoid classifying every point as an outlier (later used in the annealing heuristic), $\mathcal{L}T$ is the thin-plate splines smooth regularization, and $\mathcal{T}$ is the temperature parameter of the annealing process beginning at $\mathcal{T}_o$ and decreasing in each iteration.

$$\begin{aligned} &\underset{\mathbb{C},r,s,T}{\operatorname{argmin}} \sum_{i=1}^{n}\sum_{k=1}^{m} c_{ik}\|q_k - T(p_i)\|^2 + \lambda\mathcal{L}T - \alpha\sum_{i=1}^{n}\sum_{k=1}^{m} c_{ik} + \mathcal{T}\sum_{k=1}^{m}\sum_{i=1}^{n} c_{ik}\log c_{ik} \\ &\text{subjected to } 0 \le c_{ik}, r_i, s_k \le 1, \quad \forall i = 1,\dots,n, \quad \forall k = 1,\dots,m \\ &\qquad \sum_{k=1}^{m} c_{ik} + r_i = 1, \quad \forall i = 1,\dots,n \\ &\qquad \sum_{i=1}^{n} c_{ik} + s_k = 1, \quad \forall k = 1,\dots,m \end{aligned} \tag{6}$$

The annealing process helps to solve this optimization problem by approximating the values of the correspondence matrix and the outlier vectors, given a fixed transformation T following Eq 7 to 9. Here, u_c and v_c are the centers of mass of both sets. The approximated version of c_{ik},s_k, and r_i are finally implemented to obtain the optimal affine transformation.

$$c_{ik} = \frac{1}{\mathcal{T}}\exp\left[\frac{\alpha}{\mathcal{T}} - \frac{(q_k - T(p_i))^t(q_k - T(p_i))}{\mathcal{T}}\right], \forall i = 1,\dots,n, \quad \forall k = 1,\dots,m \tag{7}$$

$$r_i = \frac{1}{\mathcal{T}_o}\exp\left[-\frac{(u_c - T(p_i))^t(u_c - T(p_i))}{\mathcal{T}_o}\right], \forall i = 1,\dots,n \tag{8}$$

$$s_k = \frac{1}{\mathcal{T}_o}\exp\left[-\frac{(q_k - v_c)^t(q_k - v_c)}{\mathcal{T}_o}\right], \forall k = 1,\dots,m \tag{9}$$

3. Matching alternatives in corrosion pipelines: main drawbacks

The alternatives shown in the previous section address the general problem of point matching, which usually deals with image recognition like fingerprints or distortion for 3-D shapes; see, for instance, [9, 15]. This problem has also been reported for matching defects in consecutive inspections as an alternative of matching learning approaches using Support Vector Machines (SVM), decision trees, and random forest [16]. In this direction, Dann & Dann [11] adopted the approach of Yang [15] of the correspondence matrix and outlier vectors in Eq. 6.

The approach of Dann & Dann divides the pipeline into fixed segments that overlap every 0.3 m at the joints, using the points mapped into a 2D plane by unrolling the pipeline in the axial direction. The plane uses an extended version by duplicating half segments on each side, as shown in Fig. 2 to account for the pipeline continuity in the circumferential direction and to prevent any biased misclassification. This figure illustrates how those defects located from 06:00 hr to 12:00 hr (and from 00:00 to 06:00) duplicate at -06:00 hr to 00:00 hr (at 12:00 hr to 18:00 hr, respectively). Dann & Dann used an alternative version of Eq. 1 by projecting the defects in both sets to the plane $z = 1$, i.e., $a = (x_a, y_a, 1)$ and $b = (x_b, y_b, 1)$ for any $a \in \mathcal{P}$ and $b \in Q$, and using a 3×3 affine transformation T_3,

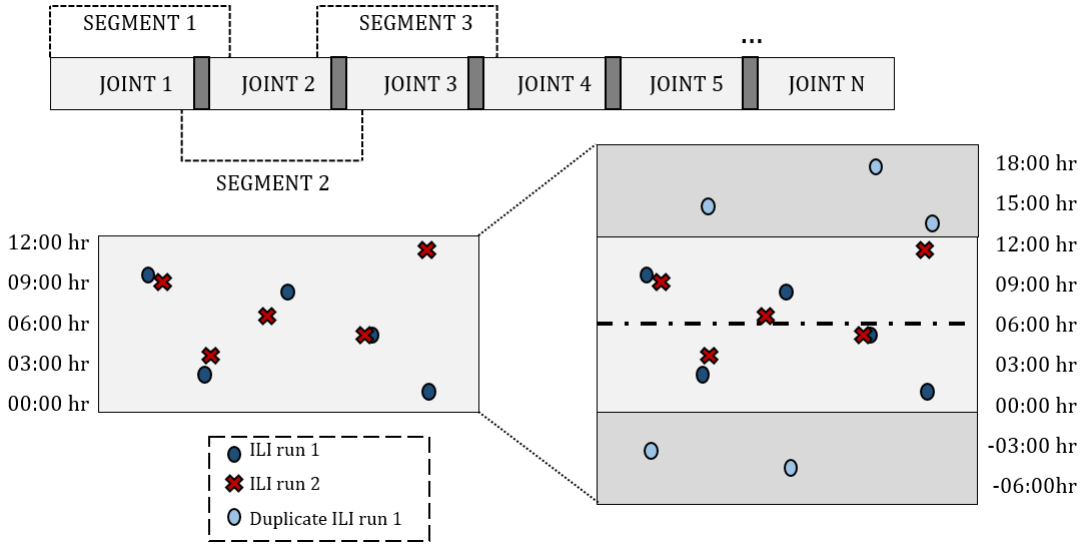

Figure 2: Scheme of the proposed matching by Dann & Dann [11].

whose components $t_{11}, t_{12}, t_{21}, t_{22}$ are associated with the scaling and rotation, t_{13}, t_{23} with the translation, and the last row vector is $[0, 0, 1]$ just to maintain the points in the same plane.

The optimization problem acknowledges the duplicates of the defects by augmenting the matrix c_{ik} and the vector r_i to $(2n \times m)$ and $(2n \times 1)$, respectively. This approach seeks for affine transformations that are not very different from I_3 (the identity 3×3 matrix) by using a controlling parameter β_c as follows $\beta_c \operatorname{Tr}\left[(T_3 - I_3)^t (T_3 - I_3)\right]$, where $\operatorname{Tr}[A]$ is the trace of matrix A. The final optimization problem is shown in Eq. 10, which is solved using again the annealing process with the temperature decreasing by $\mathcal{T} = \mathcal{T}_o \gamma^l$ with $\gamma \leq 1$ and l being the iteration step.

$$
\begin{aligned}
&\underset{\mathbb{C},r,s,T_3}{\operatorname{argmin}} \sum_{i=1}^{2n}\sum_{k=1}^{m} c_{ik}\|q_k - T_3(p_i)\|^2 - \alpha \sum_{i=1}^{2n}\sum_{k=1}^{m} c_{ik} + \beta_c \operatorname{Tr}\left[(T_3 - I_3)^t (T_3 - I_3)\right] \\
&\text{subjected to } 0 \leq c_{ik}, r_i, s_k \leq 1, \quad \forall i = 1, \ldots, 2n, \quad \forall k = 1, \ldots, m \\
&\qquad \sum_{k=1}^{m} c_{ik} + r_i = 1, \quad \forall i = 1, \ldots, 2n; \\
&\qquad \sum_{i=1}^{2n} c_{ik} + s_k = 1, \quad \forall k = 1, \ldots, m
\end{aligned}
\tag{10}
$$

This formulation seems adequate for the matching of consecutive inspections given that it considers the possibility of outliers in both sets, it seeks for a probability of matching (known as *Soft-assign*), and it prevents the trivial solution of $[c_{ik}] = \mathbf{0}$ by including the term $\alpha \sum_{i=1}^{2n}\sum_{k=1}^{m} c_{ik}$. The matching approach depends on the selection of α and β_c, where α could be linked to the outliers proportion in both sets, and β_c is a penalization parameter associated with the transformation deviation [11]. This approach assumes that both parameters are known, and the authors proposed the following feasible values: $\alpha \in [0, 0.1]$ and $\beta_c \geq 200\mathcal{T}$. However, it is noteworthy that possible matches can be misclassified as outliers by forcing a final transformation to be nearly the same as the identity matrix or assigning a lower correspondence. According to Dann & Dann, this correspondence should be greater than 0.9 to classify as a positive match. For illustrative purposes, consider the same example used in the work of Dann & Dann, and also the subset of pairs (p_i, q_k) with $p_i \in \mathcal{P}$ and $q_k \in \mathcal{Q}$ such that the nearest neighbor of p_i is q_k and vice versa. Figure 3 depicts the corresponding results based on the approach of Dann & Dann with annealing, where ILI 1 and ILI 2 depict the position from the two consecutive inspections and ILI 1 mod is the results after applying the annealing method. Note that the approach achieves a clear and good matching result when there is a marked affine transformation

(Figure 3a), in this case, a diagonal displacement in the upper right direction. However, Figure 3b shows a clear case when the transformation is barely different from the identity matrix producing a significant misclassification. The correspondence and outliers results, in this case, indicate that only 7 over 21 defects could be matched, while in the previous, case almost all of them could be paired.

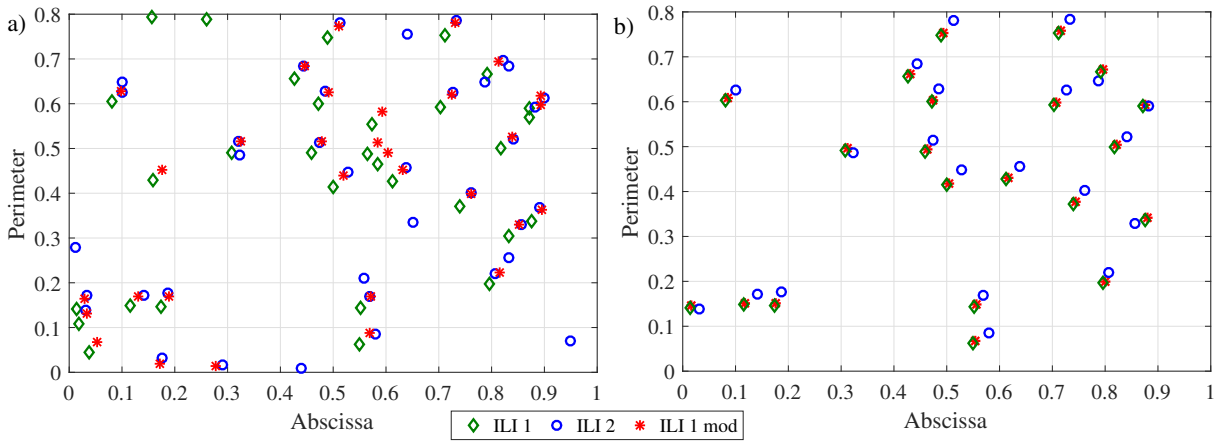

Figure 3: Point matching results with a) the example of Dann & Dann and b) a subset of points with the crossed nearest neighbors.

The point matching problem for corroding pipelines goes beyond only the affine transformation. The physical explanation of this mismatching comes from the fact that the reported defects are subjected to location uncertainties in both the axial and circumferential directions, which can be thought of as a calibrating uncertainty of the defect's position, as remarked by Pakrashi et al. [17]. Let (x, y) denote a defect, this defect would actually lie in the region $(x \pm \delta_x, y \pm \delta_y)$, where δ_x and δ_y depend on the inspection tool. For instance, following the reported by an inspection vendor [18], it can be assumed that $\delta_x = 0.1m$ and $\delta_y = 10°$ (i.e., $\frac{\pi D}{36}$, where D is the pipeline diameter). In this regard, two possible criteria can be used to identify possible matches using the region formed by $(x \pm \delta_x, y \pm \delta_y)$ or the ball centered at each defect with radius $\sqrt{\delta_x^2 + \delta_y^2}$, as shown in Figure 4. Note that ball radius can be computed only when δ_x and δ_y have the same units.

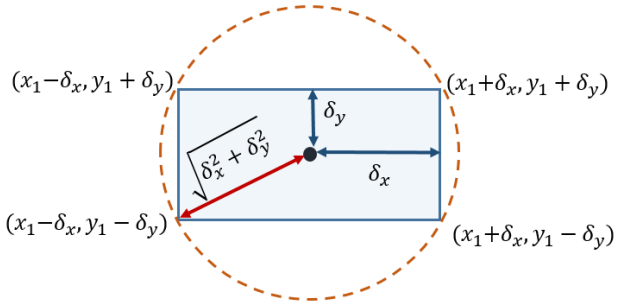

Figure 4: Location uncertainty of a defect given an axial δ_x and circumferential δ_y uncertainties position

Overall, the matching problem of corroding pipelines should also consider that some defects already have good pairing, while others relate to their nearest neighbors. Figure 5 illustrates this case using a real segment in the inner wall once the approach of Dann & Dann is applied again. This figure shows some defects with suitable preliminary matches (e.g., between km 5654 and 5655) that produce transformation with very low correspondence probabilities. This matching may be improved by omitting already detected matches, but this preprocessing would require significant manual feature selection that seeks to be avoided.

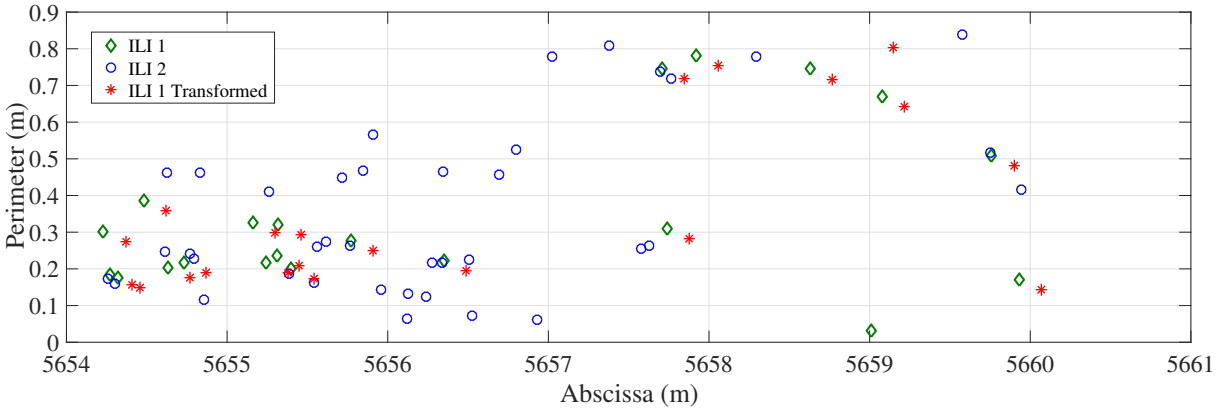

Figure 5: Possible mismatching with the approach of Dann & Dann [11].

4. Proposed approach using a Voronoi partition

This work proposes a simple approach to match the corrosion defects based on the nearest neighbor criterion between two inspections, including the possibility of outliers. For this purpose, this approach uses Voronoi cells to filter possible preliminary matches between the two inspections. Given a set of points $P = \{p_1, \ldots, p_n\}$ in $\mathbb{R}^2$, the Voronoi cell of p_l ($\mathcal{V}_l$) is defined by the subset of points in $\mathbb{R}^2$ such that the nearest point in P is p_l. For a more formal definition consider the Euclidean metric in $\mathbb{R}^2$ $d(p,q) = \sqrt{(x_p - x_q)^2 + (y_p - y_q)^2}$, then $\mathcal{V}_l = \{x \in \mathbb{R}^2 | d(x, p_l) \leq d(x, p_i), \forall i \neq l\}$. The use of the Voronoi cells allows identifying the nearest neighbors between the points of $\mathcal{P}$ and $\mathcal{Q}$ quickly, as is illustrated in Figure 6. This figure depicts the Voronoi polygons given a query, which is the closest point of $\mathcal{P}$ or $\mathcal{Q}$.

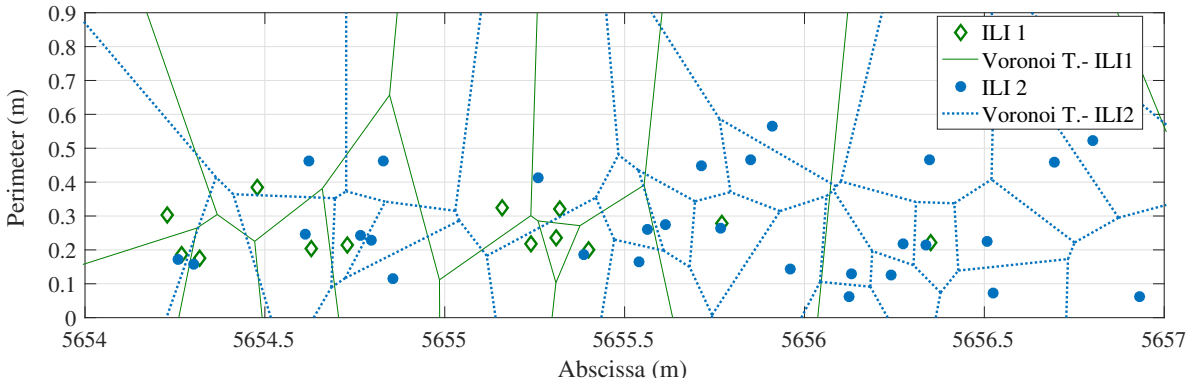

Figure 6: Voronoi tessellations from the case shown in Figure 5.

Based on the mentioned above, the approach proposes three stages to identify possible matches between two consecutive inspections (Figure 7). First, defects from two consecutive ILI measurements are preprocessed by determining their crossed nearest neighbors. Second, these nearest neighbors are implemented in an iterative process to estimate matching transformation until the transformed data converges in each iteration. Finally, the transformation determines the correspondence matrix and outliers vectors. This approach will be described in detail below[1].

[1]Note that this type of multistage approach has also been reported in defect detection [19] and spatial statistics [20]

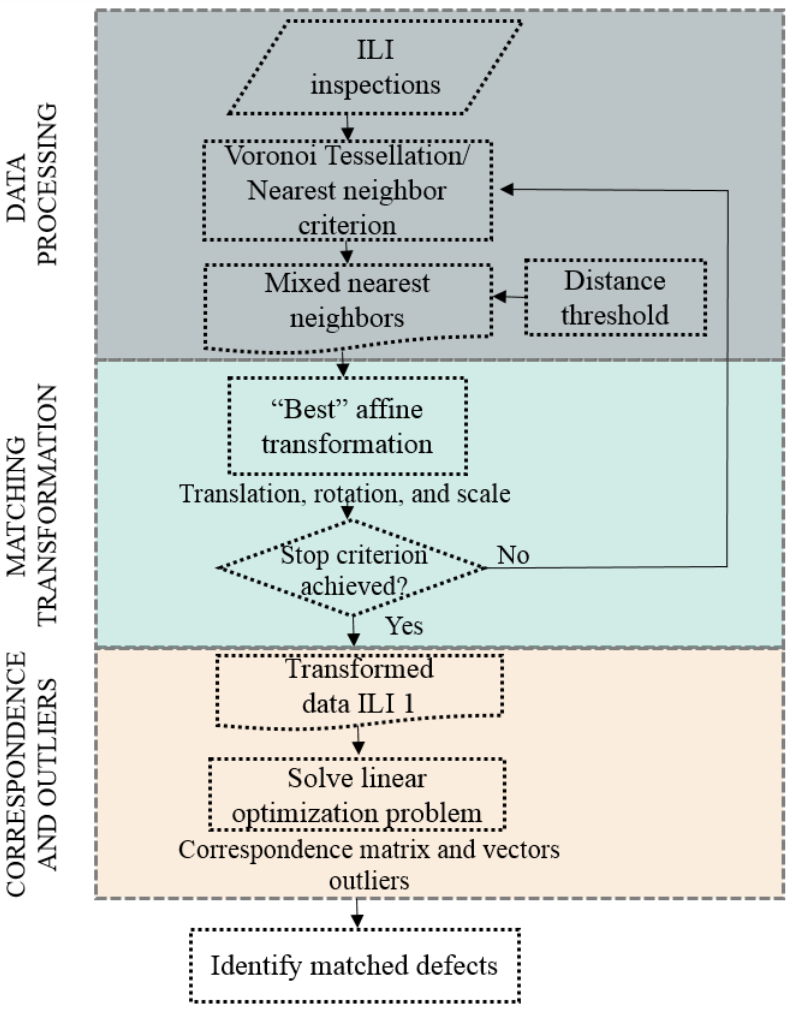

Figure 7: Proposed methodology for defects matching

4.1. Data processing

The data processing starts by duplicating each defect of the first inspection (ILI 1), as depicted in Figure 2. This duplication aims to account for the pipeline continuity in the circumferential direction, i.e., ensuring that those points at 12:00 hr continue in the 0:00 hr. Denote the number of final points in the first inspection by $2n$ and m for the second. The Voronoi cells $\mathcal{V}_1^1, \ldots, \mathcal{V}_{2n}^1$ and $\mathcal{V}_1^2, \ldots, \mathcal{V}_m^2$ are determined iteratively following any available method. Some of the common methods include the Plane-sweep, the tree expansion & deletion algorithm, or iterative approaches evaluating the dual diagram, i.e., the Delaunay Triangulation [21, 22]. This work considers the latter approach based on the functions included in the R-project package *deldir* for Delaunay Triangulation and Dirichlet (Voronoi) Tessellation. These Voronoi cells are required to be assigned to a unique tile list from 0 to $2n$ (0 to m, respectively) for the first (second) inspection to identify the tiles containing each mixed point, i.e., points sharing being the nearest neighbors, as illustrated in Figure 8. Denote by T_{l1} and T_{l2} the tile list of the mixed points, and $T_{\mathcal{V}^1}$ and $T_{\mathcal{V}^2}$ as the $2n \times m$ matrices version of these lists, as the form of an indicator matrix. For instance, if the first entry of T_{l1} is s then the first row of $T_{\mathcal{V}^2} = e_s$, where e_s is the standard unit vector of m positions with 1 in the s^{th} position and elsewhere zero. Similarly, if the first entry of T_{l2} is r, then the first column of $T_{\mathcal{V}^1} = e_r$ with 1 in the r^{th} position. The preliminary mixed nearest neighbors are determined by the Hadamard product or the element-wise product, i.e., $T_{\mathcal{V}} := (T_{\mathcal{V}^1} \odot T_{\mathcal{V}^2})_{ij} = (T_{\mathcal{V}^1})_i (T_{\mathcal{V}^2})_j$, and by considering only those pairs of defects where $d(p_i, q_k) < \delta$ where δ is

defined by $\delta = \sqrt{\delta_x^2 + \delta_y^2}$ or by the vector (δ_x, δ_y) as illustrated in Figure 4. Denote the set of nearest neighbors by (p_i, q_i) for $i = 1 : \ell \leq \min(2n, m)$, and select from the original points or the duplicate those with the lower nearest neighbor distance.

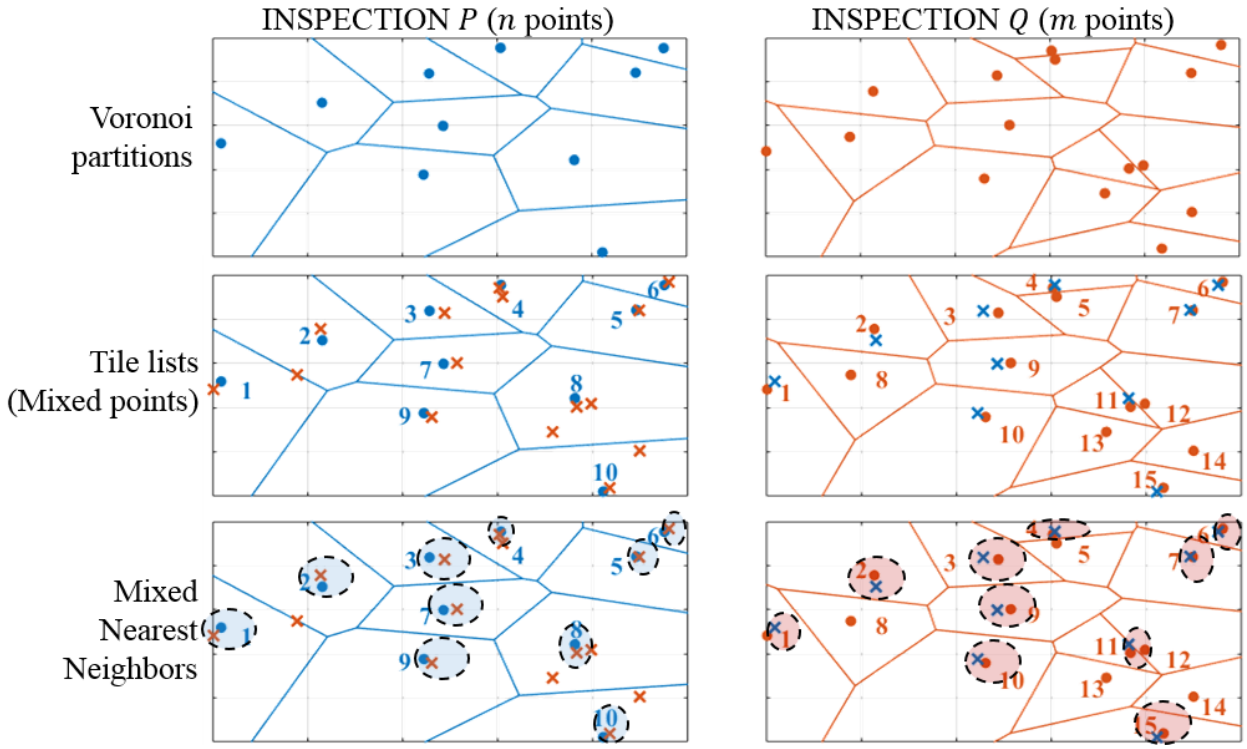

Figure 8: Scheme of the data processing.

4.2. Matching transformation approach

The second stage seeks the best feasible transformation given the initial mixed nearest neighbors obtained from both Voronoi cells. For this purpose, an iterative method is implemented following a similar procedure as reported by Besl & McKay in the Iterative Closest Point (ICP) [9]. First, the nearest neighbors are determined using the Voronoi cells, then the best affine transformation is determined following the optimal transformation reported by Chang et al. [14] and shown in Eq. 2. This transformation is applied to the data from the first inspection, and the iterative process finishes when the mean square error (MSE) of the matchings between two consecutive iterations is shorter to a predefined threshold, i.e., if $d^k = \sum_{i=1}^{\ell} \|p_i - q_i\|^2$ for the k^{th} iteration, then the stopping criterion is achieved when $\tau > \min(d^k - d^{k+1}, d^{k+1})$.

4.3. Correspondence and outliers optimization approach

The final matches are identified following the correspondence matrix and vector outliers. Given the affine transformation T_3 in Eq. 10, the optimization problem turns into linear programming with linear constraints, as shown in Eq. 11, where $w_{ik} = \|q_k - T_3(p_i)\|^2$, which may be limited to a binary solution indicating the matches and the classification as outliers in both sets [15]. Several methods can solve this linear optimization problem, but this approach uses linear programming following the package *lpSolve* of R-project due to its simplicity. Other approaches can be studied like a Benders Decomposition Method (BDM), which is an approach with an increasing interest in the field of optimization for both Linear (LP) and Mixed-Integer Linear Programming (MILP) problems; however, it is out of the scope of this work.

$$
\begin{aligned}
&\underset{\mathbb{C},r,s}{\operatorname{argmin}} \sum_{i=1}^{2n}\sum_{k=1}^{m} c_{ik}(w_{ik}-\alpha) \\
&\text{subjected to } 0 \le c_{ik}, r_i, s_k \le 1, \quad \forall i = 1,\dots,2n, \quad \forall k = 1,\dots,m \\
&\sum_{k=1}^{m} c_{ik} + r_i = 1, \quad \forall i = 1,\dots,2n \\
&\sum_{i=1}^{2n} c_{ik} + s_k = 1, \quad \forall k = 1,\dots,m
\end{aligned}
\tag{11}
$$

5. Spatial dependencies of the case study

5.1. Main parameters

The case study concerns an API 5LX52 pipeline 45km long with six main vales; its height lies between 2560 to 2660m above sea level. Near kilometer 33, there is a river crossing, whereas the last 10km are close to urban zones. The pipeline has a nominal wall thickness of 6.35mm and an external diameter of 273.1mm. The analysis presented here was based on data obtained from two consecutive ILI measurements two years apart. According to the ILI report, this diameter is maintained along the entire abscissa, while the wall thickness exhibits greater variability due to the location of welded covers, valves, dents, and manufacturing flaws. For further details, please refer to Amaya-Gómez et al. [23]. Table 1 shows a broad classification of the soil along the pipeline following the taxonomy of the USDA (United States Department of Agriculture). The pipeline has a bituminous coating of coal tar and an impressed current cathodic protection (ICCP) system.

Table 1: Pipeline segmentation based on the USDA soil classification

Segment*	Category	Classification	ID
0.00-6.66km	Complex	Pachic Melanudands (50%), Andic Dystrudepts (20%), Aeric Endoaquepts (15%), Aquic Hapludands (15%)	Soil 1
6.66-8.2km	Association	Humic Lithic Eutrudepts (35%), Typic Placudands (25%), Dystric Eutrudepts (25%)	Soil 2
8.2-9.66km	Complex	Pachic Melanudands (50%), Andic Dystrudepts (20%), Aeric Endoaquepts (15%), Aquic Hapludands (15%)	Soil 1
9.66-11.61km	Association	Humic Dystrudepts (60%), Typic Hapludalfs (40%)	Soil 3
11.61-13.48km	Complex	Pachic Haplustands (35%), Humic Haplustands (35%), Fluventic Dystrustepts (30%)	Soil 4
13.48-14.86km	Association	Aeric Epiaquents (60%), Fluvaquentic Endoaquepts (40%)	Soil 5
14.86-15.89km	Complex	Humic Dystrustepts (40%), Typic Haplustalfs (35%), Fluvaquentic Endoaquepts (25%)	Soil 6
15.89-17.62km	Association	Aeric Epiaquents (60%), Fluvaquentic Endoaquepts (40%)	Soil 5
17.62-18.65km	Complex	Humic Dystrustepts (40%), Typic Haplustalfs (35%), Fluvaquentic Endoaquepts (25%)	Soil 6
18.65-18.84km	Association	Typic Endoaquepts (40%), Aeric Endoaquepts (30%), Thaptic Hapludands (20%)	Soil 7
18.84-21.40km	Complex	Humic Dystrustepts (40%), Typic Haplustalfs (35%), Fluvaquentic Endoaquepts (25%)	Soil 6
21.40-22.63km	Association	Typic Endoaquepts (40%), Aeric Endoaquepts (30%), Thaptic Hapludands (20%)	Soil 7
26.07-27.35km	Complex	Pachic Haplustands (35%), Humic Haplustands (35%), Fluventic Dystrustepts (30%)	Soil 4
27.35-28.22km	Urban zone	-	-
28.22-30.52km	Association	Aeric Epiaquents (60%), Fluvaquentic Endoaquepts (40%)	Soil 5
30.52-33.10km	Complex	Pachic Haplustands (35%), Humic Haplustands (35%), Fluventic Dystrustepts (30%)	Soil 4
33.10-35.45km	Association	Typic Endoaquepts (40%), Aeric Endoaquepts (30%), Thaptic Hapludands (20%)	Soil 7
35.45-45.00km	Urban zone	-	-

*Both ILI did not include information of the segment from 22.63 to 26.07km

The defects measuring tool was a Magnetic Flux Leakage (MFL). Based on information reported in Amaya-Gómez et al. [24] about the inspection vendor, it can be assumed a circumferential uncertainty of 5°during the inspection. The measurement uncertainties of the defect depth, length, and width are given by $d_{ILI} = d_{real} \pm \epsilon_d$, $l_{ILI} = l_{real} \pm \epsilon_l$, and $w_{ILI} = w_{real} \pm \epsilon_w$, where $d_{ILI}, l_{ILI}, w_{ILI}$ stand for the depth, length, and width reported by the ILI tool, and $\epsilon_d, \epsilon_l, \epsilon_w$ are the measurement errors. The measurement errors can be assumed to follow normal distributions centered at 0 with standard deviations obtained from the inspection vendors [25]. It is reasonable to assume that these standard deviations are as follows: $\sigma_{\epsilon_d} = 0.1\,t$ with t the nominal wall thickness, $\sigma_{\epsilon_l} = \sigma_{\epsilon_w} = 11.70$mm, considering a

length and width accuracy of 15mm with a confidence of 80% of the data. For confidential agreements, further details of the case study cannot be provided.

5.2. Main descriptors of corrosion defects

A summary statistics of these data sets is depicted in Table 2 with the mean value and the coefficient of variation (CoV) of all the reported defects per inspection and pipe wall. Because further information about defects shape is not available in ILI, the maximum rather than the average depth for each defect will be considered from now on. Note that Table 2 show a higher CoV for the outer wall than in the inner wall that can be explained by the higher variability of corrosion factors in the soil than inside in the pipe [6].

Table 2: Summary of corrosion defects along the abscissa

Parameter	Mean (Coefficient of Variation)			
	ILI-1 Inner wall	ILI-2 Inner wall	ILI-1 Outer wall	ILI-2 Outer wall
Average depth (%t)	5.49 (0.26)	5.29 (0.27)	7.28 (0.49)	6.77 (0.46)
Maximum depth (%t)	11.54 (0.21)	11.14 (0.19)	15.84 (0.46)	14.62 (0.43)
Length (mm)	26.07 (0.49)	26.07 (0.43)	28.07 (0.48)	27.37 (0.44)
Width (mm)	22.5 (0.40)	25.92 (0.53)	28.81 (0.67)	32.60 (0.75)
Number of defects	23708	43399	2862	4264

6. Matching results and New defects identification

6.1. Matching implementation example

For a better understanding of the matching approach, the segment shown in Figure 6 is used as an example to illustrate how the matches are determined and what are the "farther matches". As mentioned in Section 4, data processing starts determining the Voronoi cells for each of the corrosion points in both inspections. Consider the example shown in Figure 6 with $n = 13$ and $m = 29$, the number of points in sets $\mathcal{P}$ and $\mathcal{Q}$. Figure 9 depicts this example, including Voronoi tile identification from 1 to 13, for the first inspection and 1 to 29 for the second. In this example, duplication is unnecessary, considering that none of the points in ILI1 were located near the border.

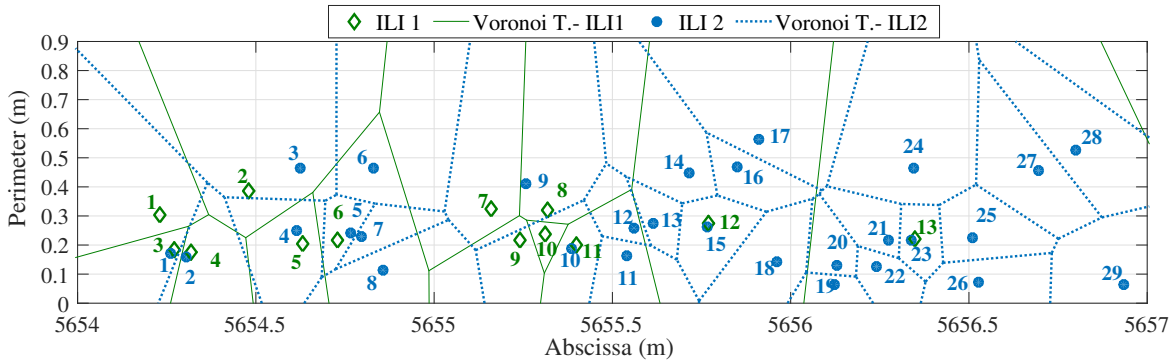

Figure 9: Voronoi tessellations and tile identification - Continuing Figure 6.

The tile list of the mixed points, i.e., the nearest neighbor in the other inspection, for the first thirteen positions are given as follows:

$$T_{l1} = \{1, 3, 1, 2, 4, 5, 9, 8, 10, 10, 10, 15, 23\}, \tag{12}$$

$$T_{l2} = \{3, 4, 2, 5, 6, 6, 6, 6, 8, 11, 11, 11, 12, ...\}. \tag{13}$$

Consequently, the 13×29 matrix version of these lists, which are determined using row and column standard unit vectors (i.e., $e_i = [0, \ldots, 1, \ldots, 0]$ at i^{th} position) follows:

$$T_{\mathcal{V}^1} = \begin{bmatrix} | & | & | & | & | & \\ e_3 & e_4 & e_2 & e_5 & e_6 & \ldots \\ | & | & | & | & | & \end{bmatrix}, \quad T_{\mathcal{V}^2} = \begin{bmatrix} — & e_1 & — \\ — & e_3 & — \\ — & e_1 & — \\ — & e_2 & — \\ & \vdots & \end{bmatrix}$$

Note that the each unit vector e_i in $T_{\mathcal{V}^1}$ have dimension 1×13, whereas each unit vector in $T_{\mathcal{V}^2}$ 29×1. The mixed nearest neighbors are determined by the element-wise product of $T_{\mathcal{V}^1}$ and $T_{\mathcal{V}^2}$ with their non-zero elements. In this example, the sparse version of this matrix, i.e., the non-zero positions, are given by $T_{\mathcal{V}} = \{(2,3), (3,1), (4,2), (5,4), (6,5), (8,9), (11,10), (12,15), (13,23)\}$, where the first position is associated with the points in ILI 1 and the second in ILI 2 that are mixed nearest neighbors. For instance, note in Figure 9 that the seventh and eighth points of ILI 1 are the closest points to the ninth point in ILI 2, but the latter is the nearest neighbor, which leads to the mixed point (8,9). These nine pairs are initially used in the optimal transformation reported by Chang et al. [14] and shown in Eq. 2. Afterward, the mixed nearest neighbors and the optimal transformation are determined iteratively until the stopping criterion of $\tau = 0.001 > \min(d^k - d^{k+1}, d^{k+1})$ is achieved, where recall that d^k is the matching MSE for the k^{th} iteration. Considering a separation greater than $\delta = \sqrt{\delta_x^2 + \delta_y^2} = 0.11m$, the final results correspond with all the mixed nearest neighbors reported at $T_{\mathcal{V}}$, except from the (2,3) pair.

Figure 10 shows the obtained results for the complete segment of seven meters long that was previously used for the annealing method (see Figure 5). This figure includes some additional "farther matches", defined as pairs with a separation greater than δ.

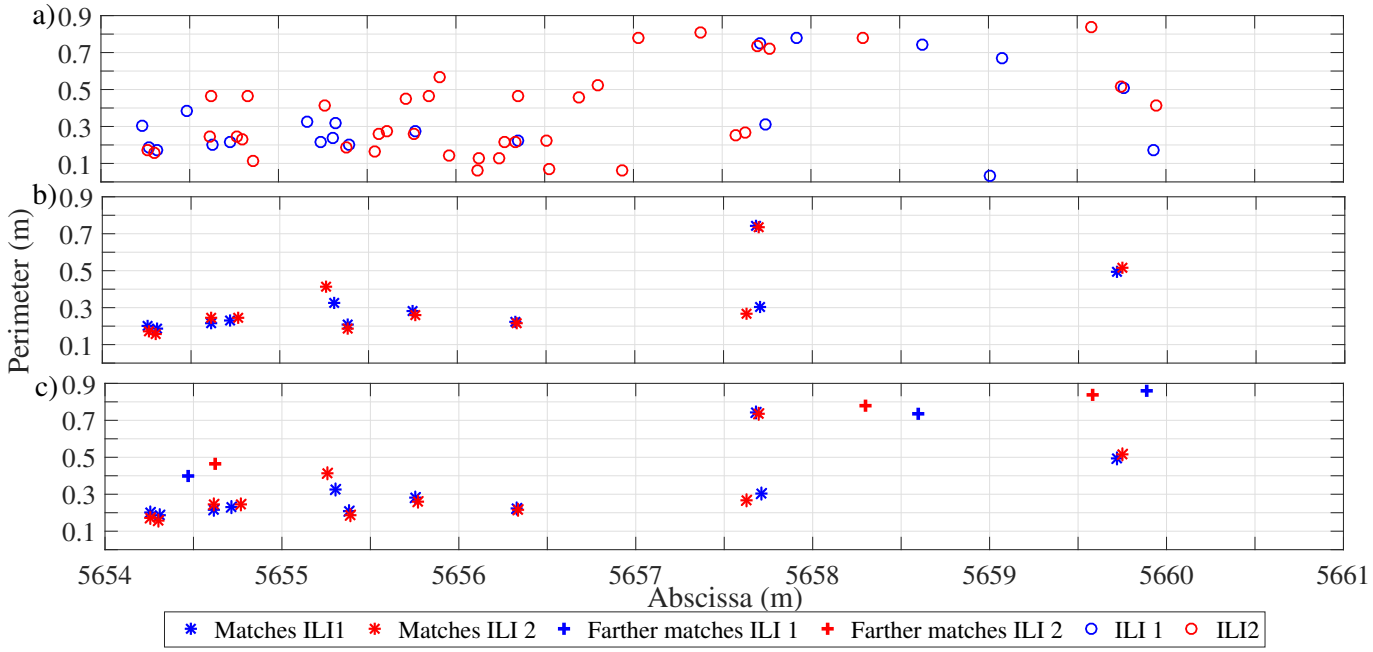

Figure 10: a) Initial ILI data; b) obtained matches by the proposed approach, and c) matches considering farther nearest defects.

In this case, Figure 10a depicts the complete segment shown in Figure 5 with the 21 and 39 defects reported for the first and second inspection, respectively. Figure 10b shows eleven matches determined with the proposed approach after transforming the data, which contrasts with the zero feasible matches in the annealing case. Finally, Figure 10c includes three possible additional matches with a larger separation, which should be further monitored. After the correspondence and outlier approach is implemented (see Eq. 11) with $\alpha = 0.01$, the matches are confirmed, and the

farther matches are considered as outliers. This parameter was considered because it obtained a higher true matching ratio for different synthetic samples.

6.2. *Comparison of the proposed matching approach with the Annealing method*

Section 4 proposed an alternative matching method based on the Voronoi tessellation and an iterative affine transformation. This approach raised as an alternative of existing methods like the Annealing method proposed by Dann & Dann [11]. This section compares both approaches using synthetic datasets. Let $n = m = 30$ and consider $\mathcal{P} := \{(p_{xi}, p_{yi})\}_{i=1}^{30}$ to be uniform random sampled in $[0, 1]^2$ and $\mathcal{Q} := \{(p_{xi} + \Delta_x, p_{yi} + \Delta_y)\}_{i=1}^{30}$ where Δ_x and Δ_y are uniform random variables associated with the location uncertainties $\delta_x = 0.1$ and $\delta_y = 10°$, i.e., $\Delta_x \sim Unif(-\delta_x, \delta_x)$ and $\Delta_y \sim Unif(-\delta_y, \delta_y)$. Consider 50 random P and Q datasets to compare both approaches using the true matching ratio. Considering that the annealing process depends on α, β_c and λ (see Section 3), a previous sensibility analysis was implemented to determine which parameters achieve the highest prediction (Table 3).

Table 3: Sensitibity analysis for the annealing matching approach

Parameter	α	β_c	λ	Matching ratio
Analysis of α	$1e^{-05}$	$200\mathcal{T}$	0.96	0.339
	$1e^{-04}$	$200\mathcal{T}$	0.96	0.342
	$1e^{-03}$	$200\mathcal{T}$	0.96	0.388
	$1e^{-02}$	$200\mathcal{T}$	0.96	0.608
	$1e^{-01}$	$200\mathcal{T}$	0.96	0.614
Analysis of β_c	$1e^{-04}$	$300\mathcal{T}$	0.96	0.340
	$1e^{-04}$	$400\mathcal{T}$	0.96	0.344
	$1e^{-04}$	$800\mathcal{T}$	0.96	0.344
	$1e^{-04}$	$1000\mathcal{T}$	0.96	0.342
	$1e^{-04}$	$2000\mathcal{T}$	0.96	0.342
Analysis of λ	$1e^{-04}$	$200\mathcal{T}$	0.9	0.346
	$1e^{-04}$	$200\mathcal{T}$	0.92	0.344
	$1e^{-04}$	$200\mathcal{T}$	0.94	0.340
	$1e^{-04}$	$200\mathcal{T}$	0.98	0.341
	$1e^{-04}$	$200\mathcal{T}$	0.99	0.341

The results in Table 3 indicate that the matching ratio increases for $\alpha \geq 0.01$, while β_c and λ do not affect the matching ratio drastically, but $\beta_c \sim 400\mathcal{T}$ and $\lambda = 0.9$ can be considered. For the proposed approach, an $\alpha \geq 0.01$ also obtained the highest true ratio, as is depicted in Figure 11.

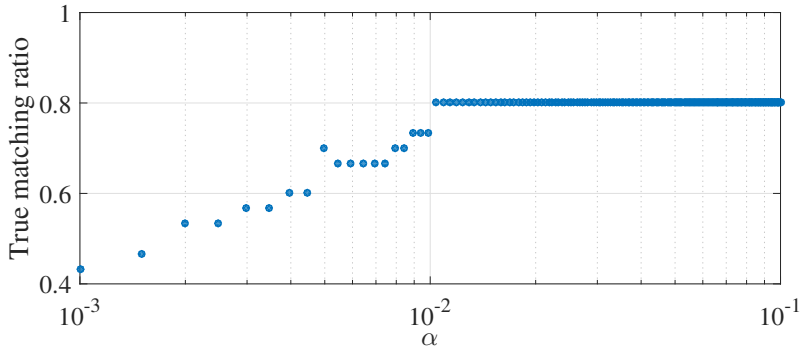

Figure 11: Sensibility analysis of α in the correspondence linear optimization in the proposed approach

Based on the above, the correct matching ratio for the annealing process using these parameters and the proposed approach are compared in Figure 12. This figure includes the results with the annealing process with the parameters

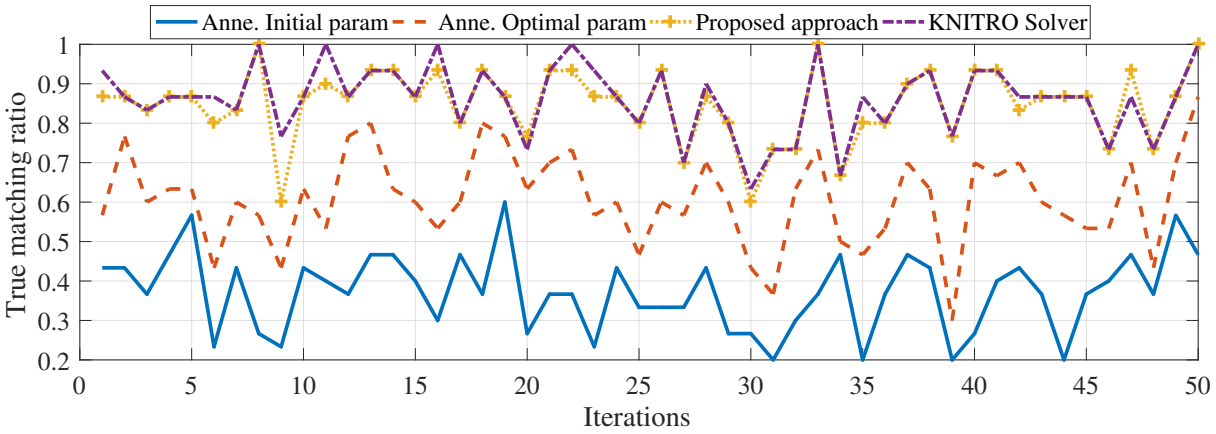

Figure 12: Comparison of the matching ratio of the proposed approach, the annealing method, and using an optimization solver

reported by Dann & Dann, i.e., $\alpha = 1e^{-04}$, $\beta_c = 200\mathcal{T}$, and $\lambda = 0.96$, and the one obtained from the sensibility analysis $\alpha = 0.1, \beta_c = 400\mathcal{T}$, and $\lambda = 0.9$.

The results indicate that the proposed approach outperforms the annealing matching almost in every case. The true mean matching for the proposed approach was 0.848 against 0.607 for the annealing process. Figure 12 also displays the true matching ratio for the solver KNITRO, which is a solver specialized for non-linear optimization problems. For this case, the optimization problem in Eq. 10 was solved using the NEOS server under an AMPL language with the parameters obtained from the sensitivity analysis. The results show similar results to those in the KNITRO solver. However, it should be highlighted that the Voronoi approach does not require any specific optimization software as in the case of AMPL, nor using a specific server or having a software license to obtain the corrosion matches. The results were obtained using the open-source software R-project, but other software alternatives are available (e.g., Python), which facilitates the implementation in practical applications. The proposed approach represents an interesting alternative for corroded pipelines based on its independence from the controlling parameters in the annealing case. Although the nearest-neighbor criterion could be affected by possible clusters (or closed neighbors), the obtained results suggest that the matching ratio was higher than in the annealing case. The latter, considering that the proposed approach focuses on an affine transformation and incorporates potential location uncertainties in both directions. This statement should be further confirmed with other synthetic and real datasets considering clustered and dispersed point patterns.

6.3. Matched defects and descriptors of new defects

The matching results allow classifying each defect as *new* or *old*, where the former refers to those defects reported only in the second inspection and the latter in both inspections. These new defects can be attributed to a miss-detection in the first inspection, a possible false alarm in the second inspection, or a purely new defect produced by the soil aggressiveness or the fluid properties. Straub [26] remarked that determining which is the reason for the appearance of these *new* defects may be impossible if the real condition of the pipeline is unknown. However, something that is certain is that there is an "indication" of new defects. This section describes the main features of both *new* and *old* sets.

The iterative approach identified both likely and farther matches in the previous example, i.e., defects with a separation higher than δ. Let us focus first on how the matching ratio, #Matches/Total points per segment, changes when the farther pairs are also contemplated. For this purpose, consider only pipe segments between consecutive joints without purely new defects (or initial mismatching), i.e., where no defects were only reported in the second inspection, and segments with possible false alarms –only records in the first inspection–. If the farther are included, the matching ratio increases from 52% to 65% for ILI1-Int and 44% to 51% for ILI2-Int, respectively. The difference is shorter for the outer wall, with an average increment from 75% to 78% for ILI1-Ext and from 65% to 68% for ILI2-Ext. Note that the matching ratio decreased for the second inspection because the number of points increased

between the two inspections. However, this difference can also be favored by the presence of clustering or "corrosion colonies". Considering the clustering criterion of ASME B31G (i.e., $3t$), about 36% and 46% of defects not being matched in the inner and outer wall are potential clusters. It indicates that the "corrosion colonies" could hide the location of these corrosion points and classify them as part of a corrosion cluster, and the "indication" is no longer available.

Table 4: Matching results based on the soil type

Soil	Matches including farther pairs				Matches without farther pairs				Number of defects*			
	Inner wall		Outer wall		Inner wall		Outer wall		Inner wall		Outer wall	
	ILI1	ILI2	ILI1	ILI2	ILI1	ILI2	ILI1	ILI2	ILI1	ILI2	ILI1	ILI2
S1	68.0%	46.2%	68.4%	63.5%	60.6%	41.1%	65.9%	61.2%	1550	2283	405	436
S2	68.6%	46.3%	NR	NR	63.8%	43.1%	NR	NR	1584	2346	0	0
S3	72.6%	48.3%	81.7%	53.8%	65.6%	43.6%	78.3%	51.6%	931	1400	60	91
S4	64.6%	43.5%	72.3%	48.5%	56.0%	37.7%	64.6%	43.3%	2774	4120	65	97
S5	66.3%	48.6%	75.0%	39.1%	59.3%	43.5%	75.0%	39.1%	5332	7268	12	23
S6	64.4%	49.1%	67.9%	43.2%	57.9%	44.2%	67.9%	43.2%	2230	2922	28	44
S7	57.6%	54.2%	59.7%	35.1%	53.8%	50.7%	56.1%	33.0%	936	994	1456	2478
UZ	58.4%	50.5%	59.1%	53.0%	52.0%	45.0%	54.9%	49.3%	7069	8167	718	800
Complete	63.1%	48.6%	61.7%	42.8%	56.6%	43.5%	58.1%	40.3%	23655	30726	2763	3985

NR. No defects reported
*Segments with possible false alarms or mismatches were not considered

The matching ratio was also compared with the different soil categories to verify if there is some relationship with the number of points (Table 4). The results indicate that the matching ratio does not change drastically at the inner wall despite the number of defects varying significantly in each soil class. For the first inspection, results ranged from around 60 to 70%, where the S3 soil had a higher rate but fewer defects. The results for the second inspection range from 40 to 55%. The outer wall presents a more significant variation, which is explained by the low number of defects in some soil classes. In both cases, the matching ratio would increase around 4 to 5% on average if potential clusters were omitted, especially soils S1 and S7.

The correspondence matrix and outliers identification contemplate all the reported defects per segment joint; however, only the matches (including the farther distances) and those defects initially not matched with a separation shorter than $\delta = 0.11m$ were considered. This filter was implemented because the remaining records would not be physically matched, and it also reduces computational time. Table 5 summarizes the matching results, ratifying 84% of the preliminary matches, discarding almost all the farther matches, and replacing them with defects initially not matched. The remaining 16% of preliminary matches were initially classified as outliers. Recall that the optimization approach in Eq. 11 produces binary outputs, which can be affected by nearly cluster segments; for instance, a defect with two close neighbors in the second inspection. In this regard, about 30% (and 38%) of the preliminary matches discarded with the correspondence matrix at the inner (outer, respectively) wall were classified as possible clusters, considering the ASME B31G grouping criterion again. Bearing in mind this limitation, the *old* defects would include both the preliminary and the final matches to recognize also the possibility of new defects from the nearest neighbor perspective.

Table 5: Matching results after applying the correspondence matrix

Dataset	Inner wall		Outer wall	
	ILI1	ILI2	ILI1	ILI2
Number of defects	23708	43399	2862	4264
Preliminary matches	12980 (84%)	12980 (84%)	1592 (83%)	1592 (84%)
Farther matches	1343 (0%)	1343 (0%)	95 (5%)	95 (5%)
Correspondence matches	12200	12200	1455	1455
Final matches	14314	14314	1714	1714

Percentage in parentheses are the matches obtained by the correspondence and outliers stage.

The *old* and *new* defects tend to be close together. The majority of *old* defects are separated less than 0.2m from

the *new* ones, as depicted in Figure 13, considering the nearest neighbor distance. The nearest *new* defects have an average depth within 11 to 12%t for both pipe walls.

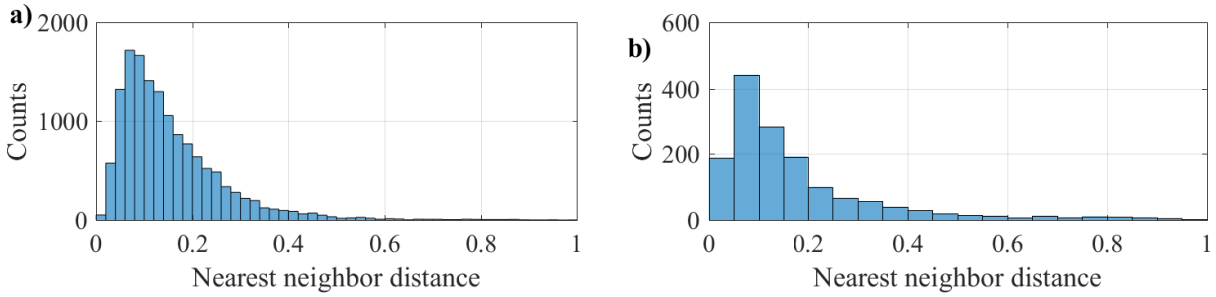

Figure 13: Nearest neighbor distance defects in *old* to *new* set for the a) inner and b) outer walls.

Table 6 shows the summary of the corrosion extent from both sets. It can be noticed that larger and wider defects appeared in the *new* defects' but with shallow depths, associated with uniform corrosion that was not initially detected in the first inspection.

Table 6: Summary corrosion extent of the *new* and *old* sets

Set	Parameter	Inner wall						Outer wall					
		Min	Q1	Q2	Mean	Q3	Max	Min	Q1	Q2	Mean	Q3	Max
old	Depth	10	10	11	11.64	12	36	10	11	14	16.8	20	70
	Length	10	18	22	25.31	30	85	10	19	24	27.47	33	109
	Width	14	18	20	26.82	30	255	16	19	28	35.69	41	270
new	Depth	10	10	10	10.89	11	36	10	10	11	13.11	14	36
	Length	10	18	23	26.44	32	92	10	19	25	27.3	33	132
	Width	12	18	20	25.47	28	271	16	18	24	30.52	35	813

7. Insights about the probability of detection and false alarm

Besides classifying each defect as *new* or *old*, the matches can be used as indicators of how the probability of detection (PoD) and the probability of false alarm (PFA) behaved for the inspection tool. Non-destructive Techniques (NDT) such as ILI deal with the possibility of detecting a corrosion defect given detection threshold, usually associated with a defect depth of $d^* = 10\%t$, where t stands for the pipeline wall thickness. This detection threshold is used as a filter to distinguish between defects that can be detected or not, and it is commonly used on one side to define the probability of detection as $PoD(d) = \mathbb{P}(d > d^*)$ [5]. The filtering process could influence the burst capacity of the corroded pipeline; however, a threshold of $d^* = 10\%t$ has been indicated to be negligible for this purpose [27]. The probability of false alarm, on the other side, represents the case of detecting a defect, although it does not exist and is linked with the noise of the inspection tool. Different researchers have implemented these probabilities to acknowledge the uncertain number of real defects. For instance, Heidary & Groth [28] proposed a population-based pitting degradation model that uses the probability of detection and the probability of false alarm (false call) to estimate the number of existing pits in the ILI measurement and those detected on a second consecutive inspection. Wang et al. [29] considered the probability of detection at a corroded pipeline rehabilitation process subjected to seismic activity.

Given a particular defect, the false detection would be related to a noise signal that produces a higher response than the detection threshold. According to Rouhan & Schoefs, these may be attributed to the surrounding conditions produced by humans' environmental conditions or the measuring process [5]. That was confirmed by Schoefs et al. [30] with an analysis of human factors accuracy and the use of protocols. These two probabilities are frequently represented with two separate probability density functions from noise and defect signals, as shown in Figure 14, which

sometimes are known as a pure noise signal, and a noise+defect signal [5]. This figure depicts that the probability of a false alarm is the area under the noise signal's curve. Besides, the probability of detection is determined by the area under the defect signal. In both cases, after the detection threshold [31].

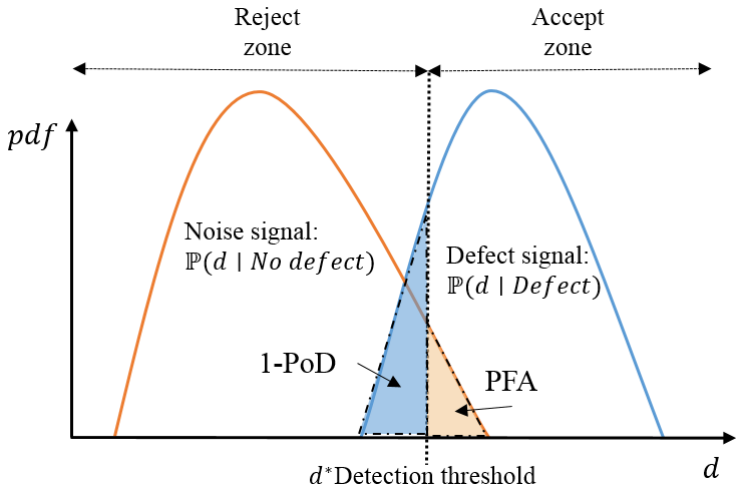

Figure 14: Defect and noise signals scheme

In the absence of the inspection signal, let us concentrate on the reported defects from the ILI measurements. If an ILI measurement occurs, the report would include a certain number of metal loss measurements roughly known as corrosion defects. These defects have a depth greater than the reporting threshold of $10\%t$; however, some questions remain unanswered: (i) Are those detected defects exist? (ii) Is there any undetected defect? These questions can be translated into the following conditional events given that a defect may be detected or not [5]:

- E1: absence of a defect, conditioned to no defect detected;
- E2: absence of a defect, conditioned to defect detected;
- E3: presence of a defect, conditioned to no defect detected; and
- E4: presence of a defect, conditioned to defect detected.

Denote the detection output by $d_e(X)$ and the existence of a defect as X. These outputs can be seen in a binary point of view, i.e., $d_e(X), X \in \{0, 1\}$; therefore, $\mathbb{P}(E_1)+\mathbb{P}(E_3) = \mathbb{P}(E_2)+P(E_4) = 1$. Following this notation, the probability of detection and false alarm can also be defined as $PoD(X) = \mathbb{P}(d_e(X) = 1 \mid X = 1)$ and $PFA(X) = \mathbb{P}(d_e(X) = 1 \mid X = 0)$. These definitions were used with the Bayes' conditional theorem by Rouhan & Schoefs to express the previous four conditional events as shown below [5]:

$$\mathbb{P}(E_1) = \mathbb{P}(X = 0 \mid d_e(X) = 0) = \frac{(1 - PFA(X))(1 - \gamma)}{(1 - PoD(X))\gamma + (1 - PFA(X))(1 - \gamma)} \tag{14}$$

$$\mathbb{P}(E_2) = \mathbb{P}(X = 0 \mid d_e(X) = 1) = \frac{PFA(X)(1 - \gamma)}{PoD(X)\gamma + PFA(X)(1 - \gamma)} \tag{15}$$

$$\mathbb{P}(E_3) = \mathbb{P}(X = 1 \mid d_e(X) = 0) = \frac{(1 - PoD(X))\gamma}{(1 - PoD(X))\gamma + (1 - PFA(X))(1 - \gamma)} \tag{16}$$

$$\mathbb{P}(E_4) = \mathbb{P}(X = 1 \mid d_e(X) = 1) = \frac{PoD(X)\gamma}{PoD(X)\gamma + PFA(X)(1 - \gamma)} \tag{17}$$

where γ is the probability of presence of a defect over the inspection section, i.e., $\gamma = \mathbb{P}(X = 1)$, so $(1-\gamma) = 1-\mathbb{P}(X = 1) = \mathbb{P}(X = 0)$ is the probability of the absence of a defect.

Normally, the PoD is a monotonically increasing function that depends on the defect depth, which can be approximated "experimentally" using the ratio of the actual number of defects over the total number of reported defects in a defect depth range [5]. Different authors have reported this approach to describe the probability of indication in a given range of interest [32]. Consider a segmentation of the depth of the defects given by $d_i, i = 0, \ldots, m$ where $d_m \leq \max(d_{ILI})$ being d_{ILI} the reported depths at the ILI measurement, whereas $d_0 = 0$ represents an intact pipeline. Accordingly, denote by n_i for $i = 1, \ldots, m$ the number of defects correctly identified by the inspection tool, over a total of N_i, for each segment $[d_{i-1}, d_i]$, then the probability of true indication (PTI) can be estimated by $PTI \sim n_i/N_i$ [32]. The problem of this approach for PoD without a field validation is that the defect's existence is assumed but cannot be guaranteed.

On the contrary, consider the event E_4, which evaluates the probability that a defect exists given it was already detected. This event was used assuming detection in both inspections[2] it does exist. Note that this approach would estimate the real number of existent defects from the first inspection; however, this assumption would neglect those repaired defects, and it may include the unlikely case where a non-existent defect was reported in both inspections. Nonetheless, this is the best approximation based on the available information considering the lack of field sampling.

The obtained results are shown in Figure 15, including exponential and log-logistic fits based on the equations depicted in Eq. 18 and Eq. 19, once the defect depth is segmented using equidistant quantiles. Similar expressions have been implemented by other authors to estimate the *PoD* such as Park et al. [33], Baskaran et al. [34], or Yazdi et al. [35].

$$f_{exp}(d) = \gamma_d \left[1 - \exp\left(\frac{-d}{\lambda_d}\right)\right], \tag{18}$$

$$f_{Logl}(d) = \frac{\exp\left(\alpha_d + \beta_d \ln(d)\right)}{1 + \exp\left(\alpha_d + \beta_d \ln(d)\right)}. \tag{19}$$

These fittings were determined using the modified nonlinear least-squares function *nlsLM* of the package *minpack.lm* in R, which incorporates the Levenberg-Marquardt algorithm. The obtained coefficients, as well as their confidence intervals and standard error, are displayed in Table 7. Overall the exponential and log-logistic functions agree very well with the "experimental" data obtained from the depth of the matched defects from the first inspection. The probability reaches 1 near 30%t deep for the inner wall, which means that any defect deeper than 30%t already detected would guarantee its presence on the inner wall. Timashev & Bushinskaya also reported a similar percentage by establishing that the probability of detection of an ILI tool is almost one [32]. For the outer wall, a depth of 30%t achieves a lower probability of 0.8, partially explained by the amount of data at the outer wall and the overall more profound defects than those located at the inner wall.

Table 7: Fitted parameters for the exponential and log-logistic function applied on the $\mathbb{P}(E_4)$

Parameters	Inner wall				Outer wall			
	Coefficient	Confidence interval		SE	Coefficient	Confidence interval		SE
		2.5%	97.5%			2.5%	97.5%	
λ_d	0.836	0.623	1.180	0.172	0.838	0.5214	1.552	0.282
γ_d	1.115	0.966	1.365	0.085	0.887	0.7185	1.301	0.110
α_d	1.320	1.211	1.438	0.050	0.541	0.4384	0.648	0.049
β_d	2.272	1.896	2.667	0.171	1.011	0.6545	1.385	0.167

Following a similar procedure, the probability of event E_2 was determined, considering the defects that could not be matched, as the counting variable n_i. As it was remarked before, the definition of E_2 and E_4 follows that $\mathbb{P}(E_2) = 1 - \mathbb{P}(E_4)$, so additional functions were not necessary, and the "experimental" results were compared with the complement of the functions obtained from Table 7 (see Figure 16). The results show a good agreement between the fitted functions and the data of the unmatched defects, although this result could be expected using the definition of the raw probability of no matches, i.e., the complement from each depth segment.

[2]Initially detected in the first inspection and latter matched with another defect from the second inspection.

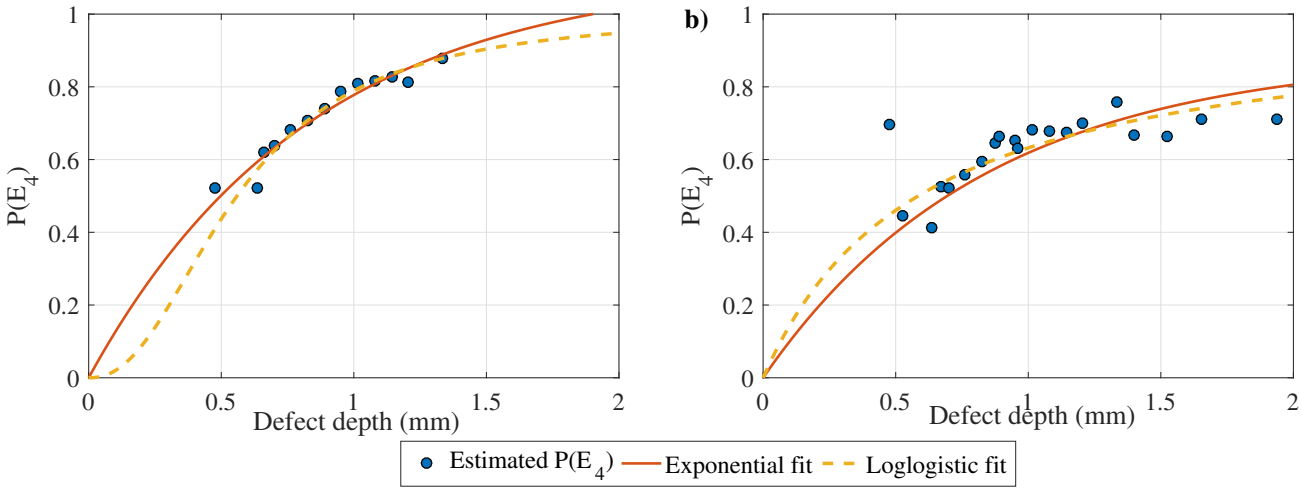

Figure 15: Estimated $\mathbb{P}(E_4)$ with the exponential and log-logistic fits for the a) inner and b) outer wall matched records in ILI1.

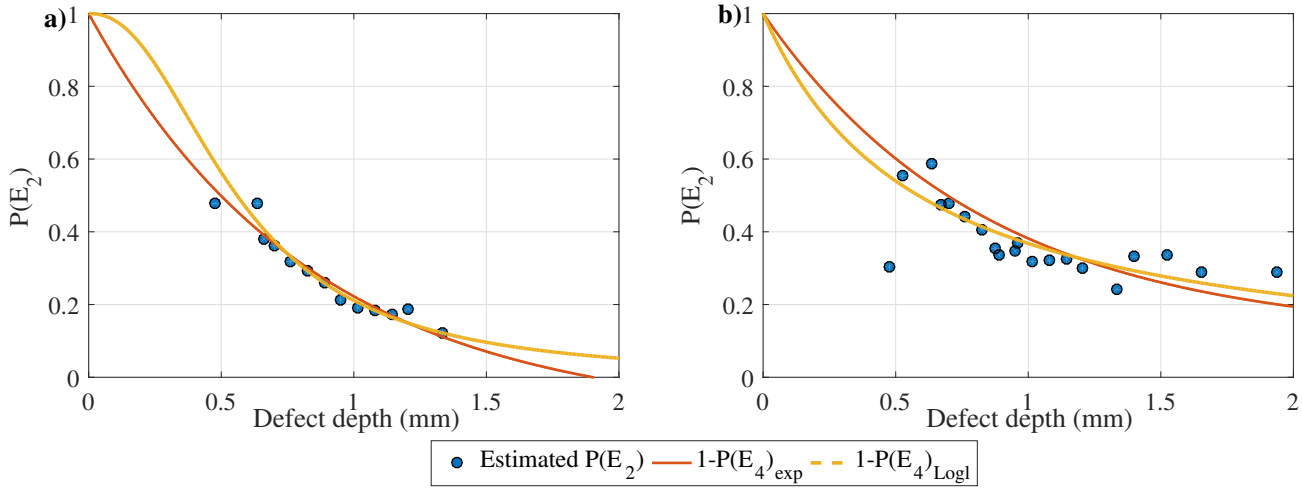

Figure 16: Estimated $\mathbb{P}(E_2)$ with the exponential and log-logistic $\mathbb{P}(E_2)$ complement fits for the a) inner and b) outer wall.

Nevertheless, this pattern is obtained regardless of the data used to fit $\mathbb{P}(E_4)$ and to calculate $\mathbb{P}(E_2)$. To demonstrate this pattern, consider a cross-validation approach using 70% of the data as a training set to determine the exponential and log-logistic fits for $\mathbb{P}(E_4)$, and the remaining 30% to estimate $\mathbb{P}(E_2)$ (test set). This procedure was implemented 100 times using random sampling, and the Mean Standard Error (MSE) from the $1 - \mathbb{P}(E_4)$ predictions and the estimates of $\mathbb{P}(E_2)$ were determined. The results shown in Figure 17 indicate that these probabilities fit quite well by obtaining an average MSE of 0.002 and 0.007 for the inner and outer wall, respectively, which confirms the results obtained in Figure 16.

Although a complete PoD description is unknown, it is commonly assumed to behave as in Eq. 18 and Eq. 19 with exponential or log-logistic fits [26, 36, 37]. Inspection vendors usually provide a reference PoD for depths from 10 to 15%t of 0.90, commonly used to fit these theoretical probabilities. For instance, Zhang & Zhou implemented the exponential version (Eq. 18) with $\gamma_d = 1$ and $q = 1/\lambda_d$, where q represents a detection capability inherent from the inspection tool. The objective is to avoid this theoretical PoD but take advantage of the probabilities of E_4 or E_2 to estimate the PoD. Recall from Eq. 17 that $\mathbb{P}(E_4)$ depends on the probability of detection, false alarm, and defect existence (γ). From these probabilities, inspection vendors commonly report a PoD reference point, whereas PFA is

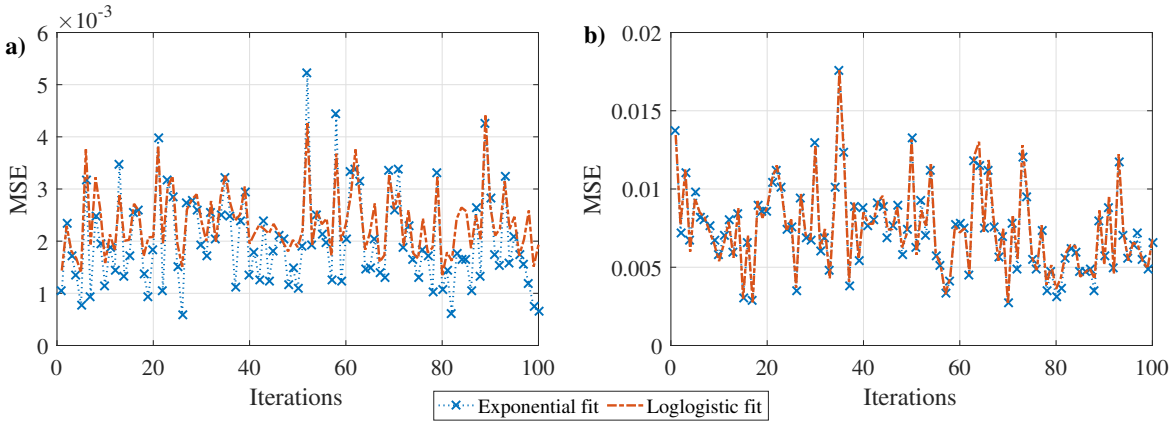

Figure 17: Mean Standard Error of $\mathbb{P}(E_2)$ and the $1 - \mathbb{P}(E_4)$ predictions under a cross-validation approach.

known to be independent and constant for the defect size [5]. Therefore, if γ is estimated, and the reference point is used, an estimate of the probability of false alarm can be solved using Eq. 17. Following Timashev & Bushinskaya, the probability of true detection and thus the existence of a defect would be at most [32]:

$$\gamma = \frac{A_d}{A_p}$$

where A_d is the surface area occupied by all the existing defects, and A_p is the total surface area being inspected. These surface areas would not contemplate the depth of the defects, and they depend on the inner and outer diameters[3] for the inner and outer walls, respectively. The existing defects were again assumed to appear in both inspections, but this probability could be higher by including additional defects. Regarding the PoD, a reference point of $PoD(15\%t) = 0.90$ was chosen based on the information reported by the inspection vendor for different MFL inspection tools.

Based on the mentioned above, the detection capabilities in each inspection, the probability of existence, and the probability of false alarm were determined for both pipe walls (Table 8). The results indicate that γ for the inner wall is about five times the probability for the outer wall, which is consistent with the number of defects and the obtained matches. However, the difference is shorter between the two obtained PFA. These false alarm probabilities are not far away from those reported by other approaches [38, 39]; however, they are specific for the inspection tool.

Table 8: Detection and existence summary results

Pipe wall	Detection Capability (q)	γ	PFA
Inner	2.42	0.2655	0.0971
Outer	2.42	0.0503	0.0291

Finally, based on the results in Table 8, the probability of detection (PoD) was estimated using the PFA, γ, and the $\mathbb{P}(E_4)$ from both pipe walls. For this purpose, each "experimental" point from Figure 15 were contemplated to solve again Eq. 17. The results are depicted in Figure 18 with green dots. This figure also includes a log-logistic fit and the expected theoretical function using the exponential fit with the detection capability. Note that the expected PoD has a clear difference with the log-logistic fit, but this difference is almost diminished after a PoD of 0.9, considering the procedure to determine both false alarm probabilities. The estimated PoD would be more conservative considering a lower detection probability that requires further tests and field validations.

This figure demonstrates that determining the probability of detection might not be straightforward; the proposed approach seeks to provide insights about PoD and PFA based on the data from consecutive inspections. Although the

[3]The inner diameter is given by $D_i = D - 2\,t_i$, where D is the outer diameter, and t is the wall thickness at the i^{th} location.

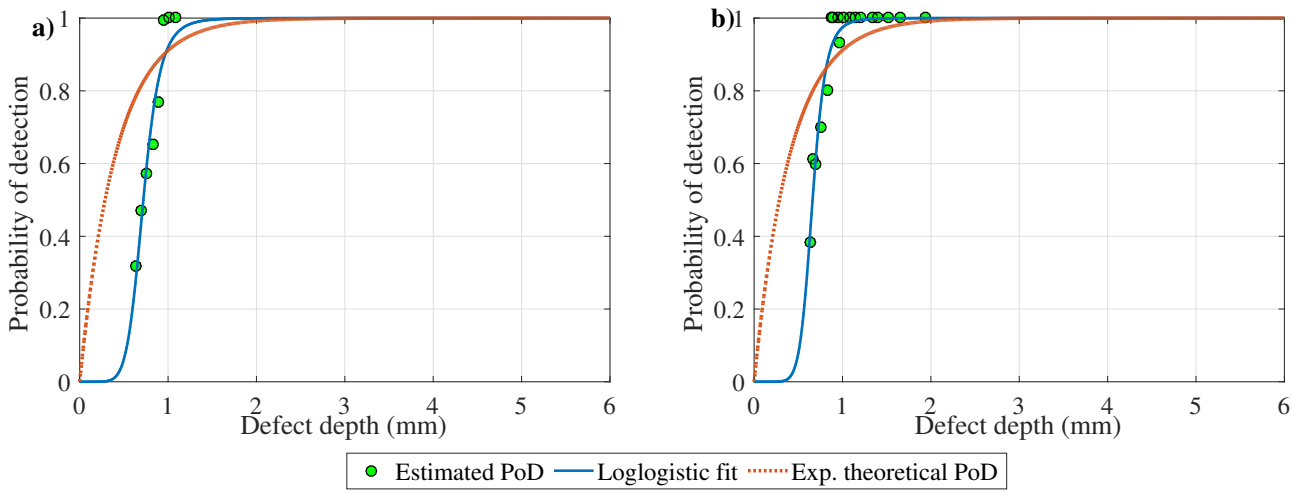

Figure 18: Estimated Probability of Detection with the complement log-logistic PoD fit and the theoretical exponential PoD for the a) inner and b) outer wall.

matching process may not identify all the existent defects in the pipeline, which could affect both $\mathbb{P}(E_4)$ and $\mathbb{P}(E_2)$, the obtained results are fair enough based on the available information. Figure 17 supports this result with the MSE outcomes under a cross-validation approach. The estimated PoD and PFA could support future intervention decisions considering whether a defect exists or not based on the defects detected by the ILI tool; for instance: 1) contemplating a predictive maintenance approach that dynamically adapts to imperfect repairs and replacements [40]; 2) quantifying how would be the economic gain by doing an inspection or a preventive maintenance [41]; and 3) predicting the distribution of corrosion defects' depth under adaptive time-dependent environmental conditions [42]. Besides, this information can be used to support reliability calculations under a noisy data context; for instance, considering a Gamma Process [43], multiple correlated defects [44], or evaluating a Spatio-temporal analysis that benefits from FEM simulations [45]. Further inspections and field validations would provide more realistic results, aiming to deal with the uncertainties inherited from the inspection tool, which, in turn, would seek to avoid unnecessary or costly repairs. Unfortunately, the inspection vendor did not provide the PoD and the PFA, but it would be interesting to compare how far they are from the predictions obtained with the matching process. Further estimates could also help to evaluate the consequence of the detection in terms of repair decisions, considering, for instance, the probability of good and wrong assessments [19, 46].

Non-destructive techniques are subjected to different types of randomness affecting the acceptance and rejection decisions of defects; PoD gives a path to evaluate the pipeline's condition, including these uncertainties. Field validations would not only allow evaluating conditional probabilities given a detection, but also the joint probabilities based on a correct detection and existence [32]:

- Probability of True Detection (PTD) $\mathbb{P}(d_e(X) = 1, X = 1)$;
- Probability of True Non-Detection (PTND) $\mathbb{P}(d_e(X) = 0, X = 0)$;
- Probability of False Non-Detection (PFND) $\mathbb{P}(d_e(X) = 0, X = 1)$; and
- Probability of False Detection (PFD) $\mathbb{P}(d_e(X) = 1, X = 0)$.

According to Timashev & Bushinskaya, these probabilities can be interpreted from a geometrical perspective by considering the area occupied by each case after a field validation [32]. Consider a pipeline segment with a length of L and diameter D, and let Figure 19 represent the output after the field validation. Consider that the black spots correspond to the defects that exist and were detected; the contoured spots with dash lines were defects not detected, but they do exist, and the light spots with continuous lines were non-existing defects reported by the inspection tool. Finally, the remaining area corresponds with an intact pipeline that was correctly not reported any defect by the inspection tool. Timashev & Bushinskaya acknowledged these probabilities by considering upper limits based on the

total area occupied and considering that $PTD + PTND + PFND + PFD = 1$, which is different from the pairs of events (E_2, E_4) and (E_1, E_3) based on the conditional definition.

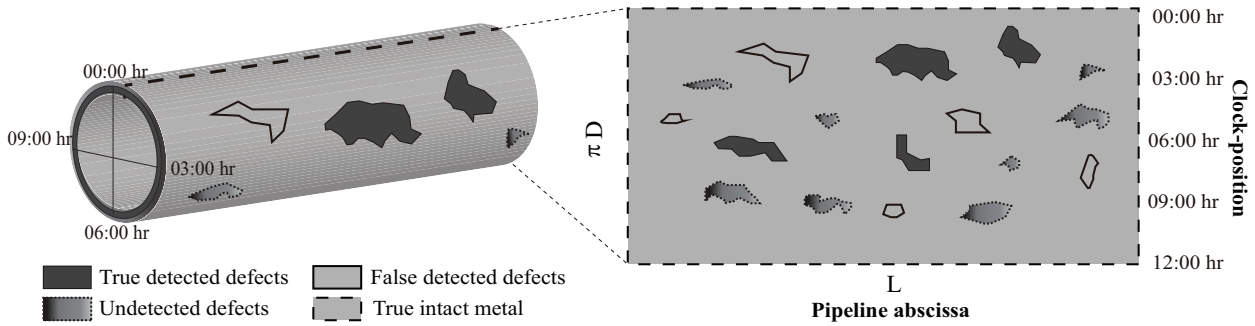

Figure 19: Scheme of a corroded pipeline condition with detected and existence results. Adapted from Timashev & Bushinskaya [32].

8. Conclusions

Pipeline integrity evaluation requires monitoring the evolution of the corrosion attack in time. Location and detection uncertainties in ILI measurements complicate this task, so a matching approach is essential. This work proposed a new approach using a Voronoi partition to filter initial possible matches, which is later implemented under an iterative approach with closed-forms "best" affine transformations and a correspondence matrix and outlier vectors optimization approach. Although pipeline operators may have more than two ILI measurements, which are helpful for corrosion growth monitoring and modeling, the proposed approach is recommended for two consecutive inspections. ILI measurements are implemented every 2 to 6 years, making the pipeline prone to maintenance or replacement procedures. This sequential approach could help follow the corrosion evolution more efficiently.

The main findings are summarized below:

1. The proposed approach focused on a transformation that contemplates the uncertain location of a corrosion defect in any direction by considering a nearest-neighbor perspective. This approach helps get competitive results than a traditional point matching problem with a defined affine transformation like the temperature annealing method.

2. Based on a segment of a real case study, this paper illustrated how the approach could identify 11 out of 21 possible matches. Based on the proposed matching, about 50% of the data could be matched between two inspections, obtaining a final number of matches of 14314 for the inner wall and 1714 for the outer.

3. The synthetic results indicated a true matching ratio for the proposed approach of 0.848 against 0.607 for the annealing case, after a sensibility analysis of their parameters. This matching ratio was also compared with an AMPL solver KNITRO in the NEOS server, obtaining similar (and even better) results. These results highlight the proposed approach as an interesting alternative for pipeline engineers that monitor the evolution of corrosion degradation.

4. Some insights about the probability of detection (PoD) and false alarm (PFA) were obtained based on the classification of *new* and *old* defects. For this purpose, the probabilities of the presence or absence of a defect given its detection from Rouhan & Schoefs [5] were implemented from an "experimental" point of view with recognized exponential and log-logistic fitting functions. The results allow us to estimate the PoD and PFA based on the reported data, which, in turn, can be implemented for further reliability analysis of the pipeline.

Acknowledgments

R. Amaya-Gómez thanks the National Department of Science, Technology and Innovation of Colombia for the Ph.D. scholarship (Grant No. 727 COLCIENCIAS in 2015) and the French Ministry for Europe and Foreign Affairs and Campus France in framework of the Eiffel Excellence Program (2018). The first author also acknowledges the valuable support of John Fontecha for implementing the KNITRO solver in the NEOS server and Juan José Torres for the discussions about the optimization resolution method.

References

[1] Y. Zhang and W.G. Weng. Bayesian network model for buried gas pipeline failure analysis caused by corrosion and external interference. *Reliability Engineering & System Safety*, 203:107089, 2020.

[2] M. Taleb-Berrouane, F. Khan, and K. Hawboldt. Corrosion risk assessment using adaptive bow-tie (ABT) analysis. *Reliability Engineering & System Safety*, 214:107731, 2021.

[3] S. Adumene, F. Khan, S. Adedigba, S. Zendehboudi, and H. Shiri. Dynamic risk analysis of marine and offshore systems suffering microbial induced stochastic degradation. *Reliability Engineering & System Safety*, 207:107388, 2021.

[4] A. Liu, K. Chen, X. Huang, D. Li, and X. Zhang. Dynamic risk assessment model of buried gas pipelines based on system dynamics. *Reliability Engineering & System Safety*, 208:107326, 2021.

[5] A. Rouhan and F. Schoefs. Probabilistic modeling of inspection results for offshore structures. *Structural Safety*, 25(4):379 – 399, 2003.

[6] R. Amaya-Gómez, E. Bastidas-Arteaga, F. Muñoz, and M. Sánchez-Silva. Statistical Soil Characterization of an Underground Corroded Pipeline Using In-Line Inspections. *Metals*, 11(2), 2021.

[7] L. Arriba-Rodriguez, J. Villanueva-Balsera, F. Ortega-Fernandez, and F. Rodriguez-Perez. Methods to Evaluate Corrosion in Buried Steel Structures: A Review. *Metals*, 8(5):334, 2018.

[8] N. Zhang, D. Zeng, Z. Zhang, W. Zhao, and G. Yao. Effect of flow velocity on pipeline steel corrosion behaviour in H2S/CO2 environment with sulphur deposition. *Corrosion Engineering, Science and Technology*, 53(5):370–377, 2018.

[9] P.J. Besl and N.D. McKay. A method for registration of 3-D shapes. *IEEE Transactions on Pattern Analysis and Machine Intelligence*, 14(2):239–256, 1992.

[10] H. Chui and A. Rangarajan. A new point matching algorithm for non-rigid registration. *Computer Vision and Image Understanding*, 89(2):114 – 141, 2003.

[11] M.R. Dann and C. Dann. Automated matching of pipeline corrosion features from in-line inspection data. *Reliability Engineering & System Safety*, 162:40 – 50, 2017.

[12] P.B. Van Wamelen, Z. Li, and S.S. Iyengar. A fast expected time algorithm for the 2-D point pattern matching problem. *Pattern Recognition*, 37(8):1699 – 1711, 2004.

[13] B.K.P. Horn. Closed-form solution of absolute orientation using unit quaternions. *Journal of the Optical Society of America*, 4(4):629–642, 1987.

[14] S-H. Chang, F-H. Cheng, W-H. Hsu, and G-Z. Wu. Fast algorithm for point pattern matching: Invariant to translations, rotations and scale changes. *Pattern Recognition*, 30(2):311 – 320, 1997.

[15] J. Yang. The thin plate spline robust point matching (TPS-RPM) algorithm: A revisit. *Pattern Recognition Letters*, 32(7):910 – 918, 2011.

[16] H. Liu, Z. Liu, B. Taylor, and H. Dong. Matching pipeline In-line inspection data for corrosion characterization. *NDT & E International*, 101:44 – 52, 2019.

[17] V. Pakrashi, F. Schoefs, J.B. Memet, and A. O'Connor. ROC dependent event isolation method for image processing based assessment of corroded harbour structures. *Structure and Infrastructure Engineering*, 6(3):365–378, 2010.

[18] ROSEN. Magnetic Flux Leakage. `http://www.rosen-group.com/global/solutions/solution-scout.html?tag_technologies=magnetic-flux-leakage`, 2014.

[19] E. Sheils, A. O'Connor, D. Breysse, F. Schoefs, and S. Yotte. Development of a two-stage inspection process for the assessment of deteriorating infrastructure. *Reliability Engineering & System Safety*, 95(3):182–194, 2010.

[20] F. Schoefs, E. Bastidas-Arteaga, T.V. Tran, G. Villain, and X. Derobert. Characterization of random fields from NDT measurements: A two stages procedure. *Engineering Structures*, 111:312 – 322, 2016.

[21] A. Dobrin. A review of properties and variations of Voronoi diagrams. Technical report, Whitman College, 2005.

[22] D.T. Lee and B. J. Schachter. Two algorithms for constructing a Delaunay triangulation. *International Journal of Computer & Information Sciences*, 9(3):219–242, 1980.

[23] R. Amaya-Gómez, E. Bastidas-Arteaga, F. Schoefs, F. Muñoz, and M. Sánchez-Silva. A condition-based dynamic segmentation of large systems using a Changepoints algorithm: A corroding pipeline case. *Structural Safety*, 84:101912, 2020.

[24] R. Amaya-Gómez, M. Sánchez-Silva, and F. Muñoz. Pattern recognition techniques implementation on data from In-Line Inspection (ILI). *Journal of Loss Prevention in the Process Industries*, 44:735 – 747, 2016.

[25] M.D. Pandey and D. Lu. Estimation of parameters of degradation growth rate distribution from noisy measurement data. *Structural Safety*, 43:60 – 69, 2013.

[26] D. Straub. *Generic approaches to risk based inspection planning for steel structures*. PhD thesis, 2004.

[27] J. Bao and W. Zhou. Influence of depth thresholds and interaction rules on the burst capacity evaluation of naturally corroded pipelines. *Journal of Pipeline Science and Engineering*, 1(1):148–165, 2021. Special Issue on Pipeline Corrosion and Its Management.

[28] R. Heidary and K.M. Groth. A hybrid population-based degradation model for pipeline pitting corrosion. *Reliability Engineering & System Safety*, 214:107740, 2021.

[29] Y. Wang, P. Zhang, X.Q. Hou, and G. Qin. Failure probability assessment and prediction of corroded pipeline under earthquake by introducing in-line inspection data. *Engineering Failure Analysis*, 115:104607, 2020.
[30] F. Schoefs, J. Boéro, A. Clément, and B. Capra. The $\alpha\delta$ method for modelling expert judgement and combination of non-destructive testing tools in risk-based inspection context: application to marine structures. *Structure and Infrastructure Engineering*, 8(6):531–543, 2012.
[31] Z. Zeng, L. Xuan, Y. Sun, L. Udpa, and S. Udpa. Probability of detection model for gas transmission pipeline inspection. *Research in Nondestructive Evaluation*, 15(3):99–110, 2004.
[32] S. Timashev and A. Bushinskaya. *Diagnostics and Reliability of Pipeline Systems*. Springer series in Reliability Engineering. Springer, 2016.
[33] K. Park, G. Lee, C. Kim, J. Kim, K. Rhie, and W.B. Lee. Comprehensive framework for underground pipeline management with reliability and cost factors using Monte Carlo simulation. *Journal of Loss Prevention in the Process Industries*, 63:104035, 2020.
[34] P. Baskaran, D.J. Pasadas, A.L. Ribeiro, and H.G. Ramos. Probability of detection modelling in eddy current NDE of flaws integrating multiple correlated variables. *NDT & E International*, 123:102499, 2021.
[35] M. Yazdi, F. Khan, and R. Abbassi. Operational subsea pipeline assessment affected by multiple defects of microbiologically influenced corrosion. *Process Safety and Environmental Protection*, 158:159–171, 2022.
[36] S. Zhang and W. Zhou. Cost-based optimal maintenance decisions for corroding natural gas pipelines based on stochastic degradation models. *Engineering Structures*, 74:74 – 85, 2014.
[37] E.S. Rodriguez and J.W. Provan. Part ii: Development of a general failure control system for estimating the reliability of deteriorating structures. *CORROSION*, 45(3):193–206, 1989.
[38] H. Wang, A. Yajima, R. Liang, and H. Castaneda. A Bayesian model framework for calibrating ultrasonic in-line inspection data and estimating actual external corrosion depth in buried pipeline utilizing a clustering technique. *Structural Safety*, 54:19 – 31, 2015.
[39] R. Howard and F. Cegla. On the probability of detecting wall thinning defects with dispersive circumferential guided waves. *NDT & E International*, 86:73 – 82, 2017.
[40] K.T. Huynh. An adaptive predictive maintenance model for repairable deteriorating systems using inverse Gaussian degradation process. *Reliability Engineering & System Safety*, 213:107695, 2021.
[41] X-X. Yuan, E. Higo, and M.D. Pandey. Estimation of the value of an inspection and maintenance program: A Bayesian gamma process model. *Reliability Engineering & System Safety*, 216:107912, 2021.
[42] K. Kim, G. Lee, K. Park, S. Park, and W.B. Lee. Adaptive approach for estimation of pipeline corrosion defects via Bayesian inference. *Reliability Engineering & System Safety*, 216:107998, 2021.
[43] I. Hazra, M.D. Pandey, and N. Manzana. Approximate Bayesian computation (ABC) method for estimating parameters of the gamma process using noisy data. *Reliability Engineering & System Safety*, 198:106780, 2020.
[44] W. Yu, W. Huang, K. Wen, J. Zhang, H. Liu, K. Wang, J. Gong, and C. Qu. Subset simulation-based reliability analysis of the corroding natural gas pipeline. *Reliability Engineering & System Safety*, 213:107661, 2021.
[45] V. Aryai, H. Baji, M. Mahmoodian, and C-H. Li. Time-dependent finite element reliability assessment of cast-iron water pipes subjected to spatio-temporal correlated corrosion process. *Reliability Engineering & System Safety*, 197:106802, 2020.
[46] E. Sheils, A. O'Connor, F. Schoefs, and D. Breysse. Investigation of the effect of the quality of inspection techniques on the optimal inspection interval for structures. *Structure and Infrastructure Engineering*, 8(6):557–568, 2012.